RMetS
Royal Meteorological Society

Mesoscale simulations of atmospheric CO_2 variations using a high-resolution model system with process-based CO_2 fluxes

M. Uebel,[a]* M. Herbst[b] and A. Bott[a]
[a]*Meteorological Institute, University of Bonn, Germany*
[b]*Agrosphere, IBG-3, Forschungszentrum Jülich GmbH, Germany*

*Correspondence to: M. Uebel, Meteorological Institute, University of Bonn, Auf dem Hügel 20, D-53121 Bonn, Germany.
E-mail: markus.uebel@uni-bonn.de

A new coupled high-resolution biosphere–atmosphere model (TerrSysMP-CO_2) is applied to simulate mesoscale and diurnal variations of atmospheric CO_2 mixing ratios. The model is characterized by process-based parametrization calculating atmospheric dynamics and biogenic processes considering the prognostically varying CO_2 content at the surface. An advanced parametrization of soil respiration is used distinguishing between heterotrophic and autotrophic respiration and explicitly considering the effect of varying soil moisture. In addition to biogenic CO_2 fluxes, high-resolution anthropogenic emissions are included in the simulations.

The model performance is verified with eddy-covariance fluxes and meteorological and CO_2 concentration measurements at various heights of a tower. It is found that a correct representation of turbulent mixing is most critical for a precise prediction of near-surface CO_2 mixing ratios and respective vertical gradients. High-resolution simulations were performed for a region with complex terrain, heterogeneous land use and densely populated areas. The relative influence of diverse land use, orography as well as of synoptic and mesoscale transport on the spatio-temporal CO_2 distribution is analyzed. The results indicate that, in regions with hilly terrain at night and in the morning, the CO_2 patterns are strongly influenced by terrain-induced local circulations. Moreover, in densely populated regions, fossil fuel emissions are an important source of atmospheric CO_2. Finally, the simulated canopy fluxes and atmospheric conditions, calculated using two different crop physiological parameter sets, are compared.

Key Words: carbon dioxide; net ecosystem exchange; biogenic CO_2 fluxes; anthropogenic emissions; photosynthesis; soil respiration; CO_2 transport; turbulent mixing

Received 5 October 2016; Revised 24 January 2017; Accepted 24 March 2017; Published online in Wiley Online Library

1. Introduction

The relevance of increasing atmospheric CO_2 contents for the estimation of future global warming is well known. Thus, an accurate quantification of the CO_2 budget and the distribution of CO_2 sources/sinks is crucial for precise climate simulations both at global and regional scales. To achieve a realistic spatio-temporal distribution of CO_2 fluxes, two contrasting approaches are used. On the one hand, in the 'top-down' method terrestrial CO_2 fluxes are derived from a combination of observed CO_2 variabilities and (global) atmospheric transport models, i.e. inverse modelling (e.g. Gerbig *et al.*, 2009; Peters *et al.*, 2010). On the other hand, in the 'bottom-up' approach field-scale observations of CO_2 exchange, e.g. eddy-covariance (EC) measurements are upscaled to derive the net CO_2 exchange of ecosystems at larger scales. However, due to several uncertainties, a large mismatch exists between local flux measurements and fluxes derived from inverse modelling (e.g. Dolman *et al.*, 2006; Ter Maat *et al.*, 2010). In particular, the representativeness of CO_2 fluxes at field scale is not necessarily guaranteed, and mesoscale atmospheric circulations influencing measured CO_2 mixing ratios are not resolved with global models used for inverse modelling (van der Molen and Dolman, 2007; Pérez-Landa *et al.*, 2007). To bridge the gap between local and global scale, this study deals with the spatio-temporal variability of CO_2 fluxes and atmospheric CO_2 mixing ratios at the mesoscale.

In the planetary boundary layer (PBL), high horizontal gradients were observed in the mesoscale CO_2 distribution in flight campaigns (e.g. Dolman *et al.*, 2006). Therefore, mesoscale models with high spatial resolutions are necessary to properly simulate these gradients caused by variable atmospheric flow

as well as by heterogeneous vegetation (Ahmadov *et al.*, 2007; Sarrat *et al.*, 2007; Smallman *et al.*, 2013; Oney *et al.*, 2015). The question arises as to the main controlling factors (e.g. land use heterogeneity, synoptic flow, mesoscale flow, anthropogenic emissions) explaining CO_2 gradients at the regional and mesoscale where limited observations are available (Nicholls *et al.*, 2004; Ter Maat *et al.*, 2010). This knowledge is required to improve the upscaling of local flux measurements to mesoscale distributions of CO_2 fluxes.

In the last decade, CO_2 mixing ratios and fluxes have been investigated with several mesoscale biosphere–atmosphere models. Nicholls *et al.* (2004) have analyzed CO_2 variations in the Great Lakes region (USA) and have identified diurnal, local and regional-scale variability caused by varying turbulent mixing and orographically induced atmospheric flows (e.g. katabatic winds). Moreover, Ahmadov *et al.* (2007) and Sarrat *et al.* (2009) have compared the results of two model systems with *in situ* (CO_2 tower, EC stations) and remote-sensing (aircraft) observations in a rather flat region in southwestern France. Both models indicate horizontal patterns in the atmospheric CO_2 distribution resulting from different dominant land use and mesoscale circulations (land–sea breezes) in that particular region. In an intercomparison study, five biosphere–atmosphere models with different levels of complexity have been compared to estimate the uncertainty of mesoscale simulations caused by different parametrization (Sarrat *et al.*, 2007). Moreover, Tolk *et al.* (2009), Ter Maat *et al.* (2010) and Smallman *et al.* (2013) have studied CO_2 fluxes and atmospheric CO_2 patterns over the Netherlands and Scotland by coupling regional atmospheric models to more advanced biosphere models.

Some of these models describe the biosphere with highly simplified diagnostic relations to satellite indices (Ahmadov *et al.*, 2007) or with idealized fluxes (Pérez-Landa *et al.*, 2007). Other studies use process-based models but with relatively coarse grid spacings ranging from 8 km (Sarrat *et al.*, 2009) to 4 km (Tolk *et al.*, 2009; Ter Maat *et al.*, 2010) which may be not appropriate for the application in regions with complex terrain. Another limitation of most studies is a coarse resolution of anthropogenic emissions, e.g. 1° (Pérez-Landa *et al.*, 2007; Ter Maat *et al.*, 2010) or 10 km (Ahmadov *et al.*, 2007; Tolk *et al.*, 2009; Sarrat *et al.*, 2009).

In contrast, in this study we developed and applied a new coupled atmosphere–biosphere model using *process-based* approaches for biosphere processes. Innovative in this study is that for soil respiration we have included RothC (Coleman and Jenkinson, 2005), a commonly applied carbon turnover model (e.g. Jones *et al.*, 2005), in the model instead of simple temperature relationships used in most former studies. Moreover, the fully prognostic spatio-temporal varying atmospheric CO_2 content is used to calculate photosynthesis and transpiration. As additional CO_2 sources we integrate very-high-resolution (1 km) time variable anthropogenic emissions into the simulations. Combined with fine grid spacings (atmospheric transport: 1.1 km, biosphere: 500 m), this model captures most relevant processes to perform precise simulations in regions with complex terrain and densely populated areas.

This study has the following objectives. The new model system is used to simulate mesoscale and diurnal variations of atmospheric CO_2 mixing ratios. For the high-resolution simulations a heterogeneous region was selected to analyze the impact of different processes (e.g. atmospheric flow, complex terrain, land use) on atmospheric CO_2 patterns and we hypothesize that mesoscale circulations induced by the topography control the spatial CO_2 distribution. The results provide valuable information for regional-scale inverse modelling using coarser grid resolutions. Moreover, by comparing simulated vertical CO_2 profiles with observations at several heights on a meteorological tower, the influence of varying intensities of turbulent mixing on the vertical CO_2 distribution is studied for different weather conditions. Finally, we show the effect of using two different plant crop physiological parameter sets on canopy fluxes and the resulting meteorological conditions in the PBL.

In section 2, the modelling system is described as well as the selected domain, lateral boundary conditions and observations used for verification. In section 3, the model results are compared with meteorological and CO_2 mixing ratio measurements and EC fluxes with a special focus on the performance in different turbulent situations. In section 4, the model is applied for the analysis of heterogeneous canopy fluxes and mesoscale spatio-temporal variations of atmospheric CO_2 mixing ratios. The results are summarized and discussed in section 5.

2. Numerical model and observations

2.1. *Numerical modelling system: TerrSysMP-CO_2*

The modelling system is based on the Terrestrial Systems Modeling Platform (TerrSysMP; Shrestha *et al.*, 2014) consisting of the regional numerical weather prediction (NWP) model COSMO (Consortium for Small-scale Modelling, version 4.21), the Community Land Model (CLM, version 3.5) and the hydrological model ParFlow. Since in this study only the atmospheric model (COSMO) is coupled to the terrestrial model (CLM), ParFlow is not further considered. Significant improvements at the regional climate scale have been shown by coupling the climate version of COSMO to the advanced land surface model CLM (e.g. Davin *et al.*, 2011; Davin and Seneviratne, 2012). In contrast, TerrSysMP couples the NWP version of COSMO to CLM. Only the most important features of TerrSysMP are described, but a more detailed description of the model components and their coupling can be found in Shrestha *et al.* (2014). The components of TerrSysMP are coupled via the coupler OASIS3 (Valcke, 2013) using the multiple-executable approach. This means that each model has its own executable, allowing different model time steps and grid spacings of each model component. For the numerical investigation of CO_2 fluxes and spatio-temporal variations of mesoscale CO_2 patterns in the atmosphere, TerrSysMP was extended by a fully prognostic two-way coupling of CO_2 between COSMO and CLM, in the following referred to as TerrSysMP-CO_2. COSMO prognostically calculates the atmospheric transport of CO_2 (section 2.1.1). The resulting time-variable atmospheric CO_2 content is used for the calculation of CO_2 assimilation and respiration by CLM (sections 2.1.2 and 2.1.3). In turn, the atmospheric CO_2 concentration is influenced by local CO_2 tendencies consisting of both biogenic net CO_2 fluxes provided by CLM, and anthropogenic emissions (section 2.1.4). A schematic of important CO_2 related interactions and submodels of TerrSysMP-CO_2 is shown in Figure 1; the abbreviations are explained below.

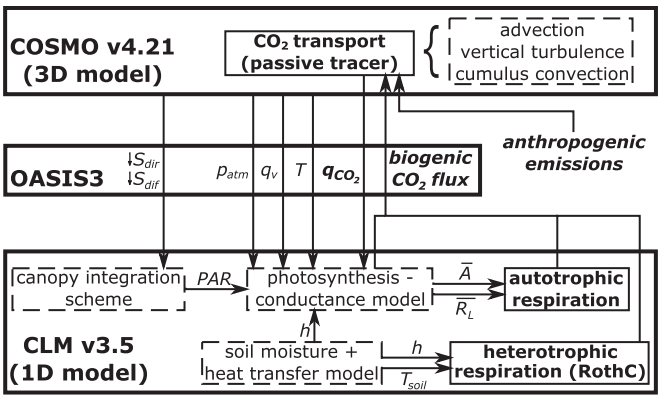

Figure 1. Schematic of the interactions between submodels of COSMO and CLM (dashed boxes) which directly influence biogenic CO_2 fluxes of TerrSysMP. Additional submodels of TerrSysMP-CO_2 (solid boxes) and coupling variables influencing fully prognostic atmospheric CO_2 are indicated by bold letters.

2.1.1. Atmospheric transport

The atmospheric state as well as the transport of CO_2 in the atmosphere (advection, turbulence, convection) is calculated by an updated version (version 4.21) of the non-hydrostatic limited-area NWP model COSMO (Baldauf *et al.*, 2011). In contrast to the original configuration, an advanced version of the positive definite one-dimensional flux-form advection scheme of Bott (1989) is used (Schneider and Bott, 2014). Vertical turbulent mixing is based on the level-2.5 scheme of Mellor and Yamada (1982) and adapted to the COSMO model (Raschendorfer, 2001). For high-resolution simulations (1.1 km), deep cumulus convection is assumed to be explicitly resolved. For the nesting simulations, the hybrid mass-flux convection scheme HYMACS (Kuell and Bott, 2008; Kuell and Bott, 2011) is used for shallow, mid-level and deep convection because at a grid spacing of 2.8 km deep convection is only partly resolved (Uebel and Bott, 2015). The transport of CO_2 mixing ratios was included as a passive fluid tracer and feedbacks on radiative transfer is neglected.

2.1.2. CO_2 assimilation and leaf respiration

CO_2 assimilation by the canopy (A^{can}) is determined with the biogeophysical parametrization of CLM (Dai *et al.*, 2003; Oleson *et al.*, 2010) coupling a biochemical photosynthesis model with a plant physiologically based stomatal conductance model. Leaf stomatal resistance (r_{st}), controlling the exchange of water and CO_2 between the leaves and the ambient air (i.e. transpiration and photosynthesis), is calculated similarly to the Ball-Berry approach as described by Collatz *et al.* (1991). The response of r_{st} (the inverse of the stomatal conductance g_{st}) to photosynthesis A and environmental conditions is parametrized by

$$g_{\mathrm{st}} = \frac{1}{r_{\mathrm{st}}} = m\frac{A}{c_{\mathrm{s}}}\frac{e_{\mathrm{s}}}{e_{\mathrm{i}}^{*}}p_{\mathrm{atm}} + g_{\mathrm{st,min}}. \quad (1)$$

In this equation, m is an empirical plant functional type (PFT)-dependent scaling factor, c_{s} and e_{s} are the CO_2 partial pressure and water vapour pressure at the leaf surface, respectively, e_{i}^{*} is the saturation vapour pressure inside the leaf at the vegetation temperature T_{v}, p_{atm} is the atmospheric pressure at the surface and $g_{\mathrm{st,min}}$ is the minimum stomatal conductance when A is zero.

When CLM is coupled to COSMO, the environmental conditions p_{atm} and e_{s} are prognostic variables provided by the atmospheric model. In TerrSysMP, e_{s} is derived from the atmospheric specific humidity (q_v) at the COSMO surface level (Figure 1). However, c_{s} is *diagnostically* calculated from a constant CO_2 mixing ratio in the ambient air. In contrast, the two-way coupling of CO_2 in TerrSysMP-CO_2 additionally includes c_{s} as a *prognostic* variable which is derived from the specific CO_2 content (q_{CO_2}) at the surface level. Thus, in TerrSysMP-CO_2, r_{st} (Eq. (1)) is not only influenced by the spatio-temporal varying atmospheric humidity, but also by varying atmospheric CO_2 contents. The stomatal control of the H_2O and CO_2 exchange between the canopy and the atmosphere is then calculated more consistently.

Leaf photosynthesis (A) is calculated with a modified version of the biochemical model of Farquhar *et al.* (1980), but with an advanced representation of the maximum rate of carboxylation ($V_{\mathrm{c,max}}$) (Thornton and Zimmermann, 2007). $V_{\mathrm{c,max}}$ controls the activity of A, e.g. the capacity utilization limitation (i.e. $0.5V_{\mathrm{c,max}}$) as upper limit of A. It is highly variable among different PFTs (Table 1). For more details on the calculation of $V_{\mathrm{c,max}}$ and A, the reader is referred to Oleson *et al.* (2010). Leaf (dark) respiration (R_{L}) was included in TerrSysMP-CO_2 as $R_{\mathrm{L}} = 0.015V_{\mathrm{c,max}}$ according to Collatz *et al.* (1991).

In CLM the upscaling from leaf level to canopy level is realized with the vertical canopy integration scheme of Thornton and Zimmermann (2007) which explicitly considers structural and functional characteristics of the canopy. This one vegetation layer scheme uses a 'two-big-leaf' approach distinguishing between sunlit and shaded leaves. Sunlit leaves receive (and absorb) unattenuated direct beam solar radiation ($\downarrow S_{\mathrm{dir}}$) and diffuse solar radiation ($\downarrow S_{\mathrm{dif}}$) whereas shaded leaves receive (and absorb) scattered diffuse solar radiation only. $V_{\mathrm{c,max}}$, A and R_{L} are calculated separately using average absorbed photosynthetically active radiation (PAR) for the two leaf types. A^{can} (and $R_{\mathrm{L}}^{\mathrm{can}}$) are then determined by multiplying by the sunlit and shaded leaf area indices L (e.g. $A^{\mathrm{can}} = A^{\mathrm{sun}}L^{\mathrm{sun}} + A^{\mathrm{sha}}L^{\mathrm{sha}}$).

Table 1. $V_{\mathrm{c,max}}$ ($\mu\,\mathrm{mol}(CO_2)\,\mathrm{m}^{-2}\,\mathrm{s}^{-1}$) at the top of the canopy (including N limitation) at $T_{\mathrm{v}} = 25^{\circ}\mathrm{C}$ for a selection of plant functional types (Figure 3).

PFT	1	7	13	15$^{\mathrm{cc}}$	15$^{\mathrm{ce}}$
$V_{\mathrm{c,max}}$	43.8	32.7	31.2	20.8	198.9

For PFT = 15, different parameter sets are used (section 4.1): 'clmcrop' (cc), 'cereal' (ce).

2.1.3. Soil respiration

CLM (version 3.5) includes a carbon–nitrogen (CN) model that can be optionally used for a prognostic calculation of the carbon and nitrogen cycles (Thornton and Rosenbloom, 2005; Oleson *et al.*, 2010). Instead of using this model for soil respiration, we integrated the RothC-26.3 (RothC) model (Coleman and Jenkinson, 2005) into CLM. This carbon turnover model simulates the decomposition of organic plant material in the mineral soil. Similar to the carbon turnover approach in the CN model, RothC utilizes a carbon (C) pool concept to calculate the decomposition by soil micro-organisms. Soil organic matter is divided into five C pools: decomposable plant material (DPM), resistant plant material (RPM), microbial biomass (BIO), humified organic matter (HUM) and inert organic matter (IOM). The decomposition of each C pool (except the fully decomposed IOM) is calculated by an exponential decay:

$$C_{i,\mathrm{new}} = C_i \exp\left\{-f(T_{\mathrm{soil}})f(h)c_{\mathrm{r}}\lambda_i\Delta t\right\}. \quad (2)$$

C_i represent the C pools DPM, RPM, BIO and HUM and $C_{i,\mathrm{new}}$ the C pools after decomposition during the time interval Δt. $f(T_{\mathrm{soil}})$ considers the sensitivity on soil temperature (T_{soil}) and $f(h)$ describes a moisture reduction depending on the soil water pressure head (h). The plant retainment factor $c_{\mathrm{r}} = 0.6$ considers the deceleration of decomposition when plants grow and λ_i are the corresponding optimum decomposition rates for pool i (adopted from Coleman and Jenkinson, 2005). Whereas the decomposition rate is independent of soil texture, the partitioning of decomposed material into CO_2, HUM and BIO depends on the clay content of the soil (Coleman and Jenkinson, 2005). Equation (2) is solved for the CLM soil layers $l = \{1, \ldots, 7\}$ (0–83 cm depth). The sum of CO_2 produced in this process is released to the atmosphere as heterotrophic respiration (R_{hetero}).

For the sensitivity of microbial activity on T_{soil} ($f(T_{\mathrm{soil}})$) and on soil moisture ($f(h)$), the assumptions of Šimůnek and Suarez (1993) are used. $f(T_{\mathrm{soil}})$ is described by an exponential dependency formulated as

$$f(T_{\mathrm{soil}}) = \exp\left\{\frac{\ln Q_{10}}{10}(T_{\mathrm{soil}} - T_{\mathrm{ref}})\right\}. \quad (3)$$

T_{ref} is the reference temperature of RothC (9.25 °C) where $f(T_{\mathrm{soil}}) = 1.0$ and we assume $Q_{10} = 2.1$, leading to realistic respiration rates at soil temperatures that usually occur in the

temperate zone. Moisture reduction is expressed as:

$$f(h) = \frac{\log|h| - \log|h_1|}{\log|h_2| - \log|h_1|} \qquad h \in [h_2, h_1], \tag{4a}$$

$$f(h) = \frac{\log|h| - \log|h_3|}{\log|h_2| - \log|h_3|} \qquad h \in [h_3, h_2], \tag{4b}$$

$$f(h) = 0 \qquad h \in [-\infty, h_3] \cup [h_1, +\infty]. \tag{4c}$$

In Eq. (4) $h_2 = -1\,\mathrm{m}$ is the pressure head for optimal soil respiration, $h_3 = -10^5\,\mathrm{m}$ is the pressure head when production ceases, and h_1 is equal to the air entry pressure. h_1 depends on the soil texture and is diagnostically predefined in CLM for the given soil type. The values of h_2 and h_3 are adopted from Suarez and Šimůnek (1993). Eqs. (3) and (4) are solved for each CLM soil level l.

The initial partitioning of total organic carbon (TOC) into the RothC pools is obtained by the pedotransfer functions of Weihermüller *et al.* (2013), assuming equilibrium dependent on the clay content and the TOC content only. We use TOC profiles measured at more than 500 locations within the model domain, provided by the Landesamt für Natur, Umwelt und Verbraucherschutz Nordrhein–Westfalen (LANUV, 2012). By averaging all measurements having the same land use, representative TOC depth profiles were determined for each PFT which were linearly interpolated to the soil levels of CLM (Uebel, 2016, gives more details). The main advantages of this method are the elimination of a model spin-up, linked with tremendous computational costs, and the application of *measured* TOC profiles instead of a *simulated* equilibrium carbon distribution (final result of the spin-up) as is needed for the CN model.

In forests, above-ground litter and the forest floor (O horizon) are further C pools. The decomposition (R_O) is calculated with the same equations as for the mineral soil (Eqs (2)–(4)). The ground temperature (T_g) is used instead of T_soil, clay is set to zero and h of the uppermost soil layer is used. With the relationships of Zhang *et al.* (2008), the decomposition rates of litter and in the O horizon were estimated as $\lambda_\mathrm{litter} = 0.4\,\mathrm{year}^{-1}$ and $\lambda_\mathrm{O} = 0.13\,\mathrm{year}^{-1}$, respectively. We assume a TOC content of $9.0\,\mathrm{t\,ha}^{-1}$ for above-ground litter and $19.8\,\mathrm{t\,ha}^{-1}$ for the O horizon as found in an analysis of the Hessisches Landesamt für Umwelt und Geologie for forests in Hesse, Germany (Wegener, 2008).

Additionally, we developed a rather simple relationship between (below-ground) autotrophic respiration (R_auto) and mean rates of canopy photosynthesis and leaf respiration ($\overline{A^\mathrm{can}}$, $\overline{R_\mathrm{L}^\mathrm{can}}$). It is based on the assumption of Ryan (1991) who pointed out that total plant respiration ($R_\mathrm{L}^\mathrm{can} + R_\mathrm{auto}$) is about 50% of photosynthesis for many plant species, i.e.

$$\overline{R_\mathrm{auto}} = 0.5\overline{A^\mathrm{can}} - \overline{R_\mathrm{L}^\mathrm{can}}. \tag{5}$$

$\overline{A^\mathrm{can}}$ and $\overline{R_\mathrm{L}^\mathrm{can}}$ are monthly means, determined by a 1 year simulation of CLM driven with hourly COSMO-DE (2.8 km grid resolution) analyses for the year of interest. A linear interpolation between two months leads to $\overline{R_\mathrm{auto}}$ for the simulated day. Optionally, it would also be possible to simulate daily or weekly mean autotrophic respiration with Eq. (5). Moisture variability is taken into account by the moisture reduction factor r_auto which is determined by vertically averaging Eq. (4) weighted with the effective root fraction $e_\mathrm{root}(l)$ of each CLM soil level l:

$$r_\mathrm{auto} = \sum_{l=1}^{10} \left\{ f(h,l)\, e_\mathrm{root}(l) \right\}. \tag{6}$$

Finally, to obtain the actual autotrophic respiration (R_auto) adjusted with the actual moisture conditions in the root zone,

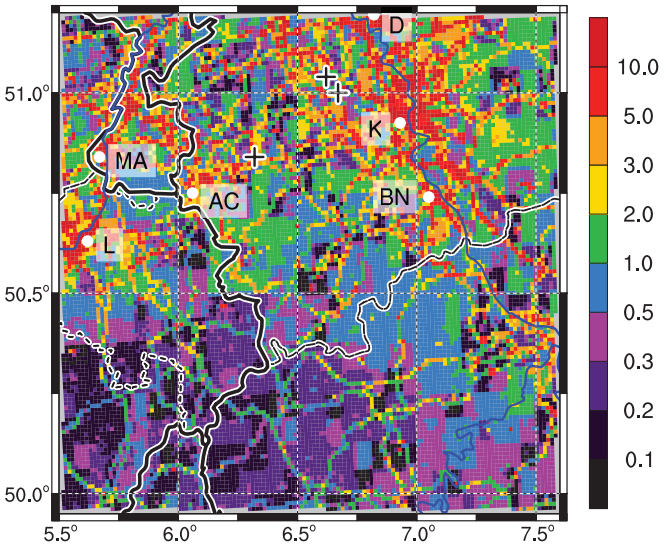

Figure 2. Annual sum of all anthropogenic emissions ($\mathrm{kg\,m}^{-2}$) as used in TerrSysMP-CO_2 including the locations of the three biggest power plants in NRW (+). Abbreviations for the cities are given in Figure 3.

$\overline{R_\mathrm{auto}}$ is normalized with the monthly mean reduction $\overline{r_\mathrm{auto}}$ and then multiplied by the actual moisture reduction r_auto:

$$R_\mathrm{auto} = r_\mathrm{auto}\left(\overline{R_\mathrm{auto}}/\overline{r_\mathrm{auto}}\right). \tag{7}$$

In summary, compared to similar model systems, an advanced parametrization of soil respiration is included in TerrSysMP-CO_2 distinguishing between heterotrophic and autotrophic respiration. In previous models, total soil respiration has been either diagnostically determined by constant fluxes for different land-use classes (Pérez-Landa *et al.*, 2007) or by simple functions of R_soil on temperature, e.g. a linear relation (Ahmadov *et al.*, 2007; Pillai *et al.*, 2011), a Q_{10} function (Sarrat *et al.*, 2009), or the approach of Lloyd and Taylor (1994) (Tolk *et al.*, 2009; Ter Maat *et al.*, 2010). In contrast, we additionally consider the effect of varying soil moisture and apply the novel concept of using measured TOC profiles for the calculation of R_hetero.

2.1.4. *Anthropogenic emissions*

In addition to biogenic CO_2 fluxes, anthropogenic CO_2 emissions strongly influence the atmospheric CO_2 content. We use a preliminary version of the TNO-CAMS CO_2 inventory, being consistent with an updated version of the TNO_MACC_II emission inventory (based on Kuenen *et al.*, 2014), provided by the Netherlands Organisation for Applied Scientific Research, TNO (H. Denier van der Gon, personal communication, 2013). This high-resolution gridded dataset is based on yearly official national reports of emitted air pollutants. The emissions are split into several Source Nomenclature for Air Pollution (SNAP) sectors; among these power generation, non-industrial combustion, industrial combustion, road transport, other mobile sources and waste treatment are relevant CO_2 sources.

For Central Europe the data were further disaggregated to a resolution of 1.0 km by the Rheinisches Institut für Umweltforschung an der Universität zu Köln (P. Franke, E. Bem and J. Klimpt, personal communication, 2013) by applying high-resolution proxy data containing information on the geographical locations of emissions of each SNAP sector. Figure 2 shows the emissions of the inner domain of TerrSysMP-CO_2 (section 2.2.1).

Each SNAP sector has a characteristic temporal variability depending on the season of the year, the day of the week and the time of the day, e.g. non-industrial combustion is distinctly higher in winter than in summer, whereas road transport mainly depends on the time of the day and on the day of the week. To account for these temporal variations, the emission time factors used in the

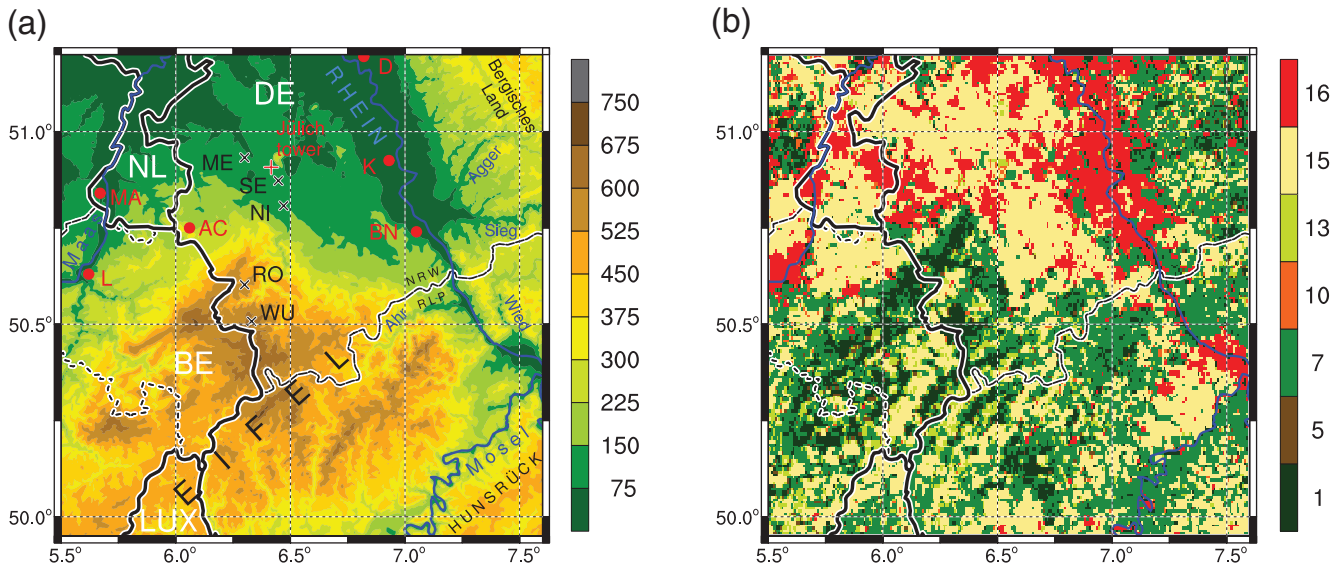

Figure 3. Characteristics of the model domain. (a) surface height (m) with German place names. The cities (red dots) are Aachen (AC), Bonn (BN), Cologne (Köln, K), Dusseldorf (D), Liège (L) and Maastricht (MA). Additionally marked are the Jülich (meteorological) tower (red +) and the EC stations (×): Merzenhausen (ME), Selhausen (SE), Niederzier (NI), Rollesbroich (RO), and Wüstebach (WU). (b) CLM plant functional types: **1** temperate evergreen needleleaf (9.7% land cover) and **5** broadleaf trees (1.3%); **7** temperate deciduous broadleaf trees (30.8%); **10** broadleaf shrub (2.3%); **13** C_3 grass (5.4%); **15** agriculture (36.6%); **16** urban areas (13.5%).

LOTOS-EUROS chemistry-transport model (Schaap *et al.*, 2005) are applied for each of the CO_2 emitting SNAP sectors. This results in hourly anthropogenic emissions which are used as additional source of atmospheric CO_2 to be read in COSMO. To consider the elevated release and additional plume rise of industrial and power plants, these emissions are vertically spread between model levels 43 and 47 ($\approx$95–500 m). In general, very detailed spatio-temporal information on anthropogenic emissions and their genesis is available for the numerical simulations.

2.2. *Experimental set-up*

2.2.1. *Model domain and grid spacings*

For high-resolution mesoscale simulations of atmospheric CO_2 mixing ratios, the atmospheric component of TerrSysMP-CO_2 (COSMO) uses a rotated spherical grid with a horizontal grid spacing of 0.01° ($\approx$1.1 km). In the vertical a stretched grid of 50 model layers is used, starting with a layer thickness of 20 m at the surface. This ensures a relatively high vertical grid resolution in the PBL with 8 and 16 layers below 500 and 2000 m, respectively. To account for the high spatial heterogeneity of the land surface, the vegetation and soil model component (CLM) has a smaller horizontal grid size of 0.005° × 0.00775° ($\approx$500 m, regular geographical coordinates, lat/lon). The soil hydrological processes are calculated by CLM using a stretched vertical grid of ten levels down to a depth of 287 cm.

The domain covers an area of 167 × 167 km (150 × 150 COSMO grid points) including the western part of Germany (DE, Deutschland), parts of Belgium (BE), the Netherlands (NL) and Luxemburg (LUX). This region is very heterogeneous in orography, land use and anthropogenic emissions (Figures 3 and 2). In the central and southern part, the domain is characterized by the hilly terrain of the Eifel with several mountain ridges separated by narrow valleys (Figure 3(a)). Further mountainous regions are east of the rivers Rhine (Rhein) and Moselle (Mosel) (i.e. Bergisches Land, Hunsrück). In contrast, in the northern and northwestern part, the terrain is predominantly flat.

Figure 3(b) depicts the land cover in terms of PFTs of CLM based on MODIS land cover data (Shrestha *et al.*, 2014). In mountainous regions and in the Moselle valley the vegetation is dominated by broadleaf and needleleaf forest and by some grassland. The flat terrain is mainly characterized by agriculture and urban areas, the latter having a rather high fraction in this particular domain (13.5%). For all PFTs the predefined monthly values of leaf and stem area index (LAI and SAI) of Shrestha *et al.* (2014) are used. The classification of the soil is based on the FAO-UNESCO (1975) Soil Map of the World as used in the external parameter set of the operational COSMO model. The predominant soil texture is loam followed by sandy loam (e.g. Rhine valley, Belgian Eifel) and sand (northwestern domain). Small areas are classified as clay-loam.

Along the river Rhine is one of the highest population densities of Central Europe; Bonn, Cologne and Dusseldorf are in this region. Further urban regions are Maastricht, Aachen and Liège (Figure 3). This is reflected in high anthropogenic emissions (cf. Figure 2) mainly caused by urban traffic, residential and industrial combustion. In contrast, in the rural Eifel region anthropogenic emissions are low. By far the highest CO_2 emissions are produced by three lignite-fired power plants ('+' in Figure 2) in North Rhine-Westphalia (NRW), being responsible for about one third of all fossil fuel burning in NRW, as well as by power plants along the river Maas.

2.2.2. *Initialization and lateral boundary conditions*

As for all limited-area NWP models, TerrSysMP-CO_2 needs initial conditions (ICs) and lateral boundary conditions (LBCs) for standard atmospheric state variables in COSMO as well as for CO_2 mixing ratios. For this, the inner domain is nested into larger domains having a grid spacing of 0.025° ($\approx$2.8 km) both for COSMO and CLM. The grid spacing is rather fine compared to other studies which use grid sizes of 6 to 48 km for their nesting domains (e.g. Ahmadov *et al.*, 2007; Tolk *et al.*, 2009; Ter Maat *et al.*, 2010, and others). Depending on the predominant direction of the atmospheric flow, three different nesting domains provide LBCs for the inner domain (Figure 4). The domains are large enough to ensure that at a moderate atmospheric flow ($\approx$ 10 m s^{-1} in the lower atmosphere), in a 24 h forecast the PBL of the inner domain is not influenced by lateral boundary effects of the outer domain. The nesting simulations are driven by hourly COSMO-EU model analysis data (grid size: 0.0625°) provided by the DWD and by hourly anthropogenic emissions. Similar to Ter Maat *et al.* (2010), atmospheric CO_2 is initialized as horizontally (and vertically) homogeneous mixing ratios adjusted to the actual atmospheric mean of the considered

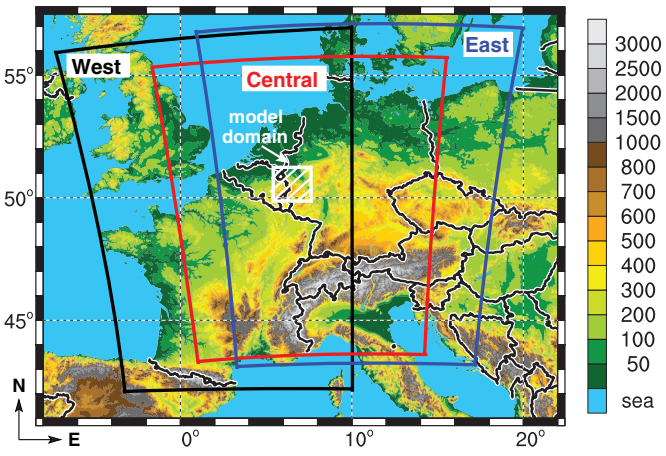

Figure 4. Surface height (m) and model nesting domains depending on the predominant direction of the atmospheric flow. The domains occupy 600 × 400 (West), 500 × 400 (Central) and 560 × 425 (East) grid points having a lat/lon grid spacing of 0.025°. The rotated north poles are the same as for the inner domain.

day being derived from the mean seasonal CO_2 variation, measured in 102.5 m height on a tower in Jülich (section 2.3).

For the case-study analyzed in section 4, the nesting simulation is started with a lead time of 24 h to the high-resolution run in order to provide a reasonable heterogeneous three-dimensional CO_2 distribution as IC for the inner domain. The nesting simulation is started at 1800 UTC because at this time of the day the horizontally and vertically homogeneous CO_2 distribution is a good approximation of the real CO_2 distribution due to a deep and well-mixed PBL (Tolk *et al.*, 2009). The simulation of the period investigated in section 3 is initialized with the same method. However, without nudging or other data assimilation methods (which inhibit a free model prediction) this 8-days period has to be split into several short-time simulations. For each of the consecutive simulations, the simulated atmospheric CO_2 fields of the previous runs are used as IC of atmospheric CO_2 mixing ratios. The nesting runs are restarted every 24 h to ensure that the initial CO_2 distribution resulting from the *predicted* meteorological situation does not deviate too strongly from the meteorological fields of the COSMO-EU *analyses* driving the model.

For the initialization of CLM, a multi-year model spin-up is required. For that, CLM was run stand-alone for 7 years, driven by hourly COSMO-DE analyses, until a dynamical equilibrium was reached. This spin-up provides realistic soil moisture and temperature profiles needed for the calculation of soil water dynamics and heat transfer in the soil as well as all other state variables needed for CLM.

2.3. *Observations*

The model performance is analyzed by comparing the simulation results with EC measurements of latent (LH) and sensible (SH) heat fluxes and CO_2 fluxes. The EC stations are mapped in Figure 3(a) (×): Merzenhausen (ME, 93 m asl, agriculture), Selhausen (SE, 105 m, agriculture), Niederzier (NI, 102 m, grassland), Rollesbroich (RO, 515 m, grassland), Wüstebach (WU, 610 m, spruce forest). All EC stations were equipped with the LI-7500 Open Path Gas Analyzer (LI-COR Biosciences, Lincoln, USA) measuring high-frequency CO_2 and H_2O mixing ratios as well as with the CSAT3 3D sonic anemometer (Campbell Scientic, Logan, USA). For the verification of TerrSysMP-CO_2, 30 min quality flagged averages are used (Mauder *et al.*, 2013) to filter out unrealistic CO_2, LH and SH fluxes. Moreover, at the Selhausen site soil respiration was measured with the LI-8100 Automated Soil Gas Flux System (LI-COR).

Additionally, meteorological and CO_2 mixing ratio measurements were made on the 124 m tall tower of the Forschungszentrum Jülich GmbH, referred to below as the Jülich tower (red ✚). The tower is located at the eastern side of a 90 m × 40 m wide clearing surrounded by a small and about 25 m tall broadleaf forest. Most of the surrounding flat terrain is characterized by arable land use. The Jülich tower has seven platforms (12.5, 20.0, 32.5, 52.5, 82.5, 102.5, 120.0 m) equipped with meteorological instruments. Similar to observations at Cabauw (The Netherlands; Tolk *et al.*, 2009) or at Beromünster (Switzerland; Satar *et al.*, 2016) we measured CO_2 mixing ratios at several heights. Three LI-840A CO_2/H_2O Gas Analyzers (LI-COR) were installed at 12.5, 32.5 and 52.5 m height. At 102.5 m above ground level (agl), the Fast Greenhouse Gas Analyzer CO_2 CH_4 H_2O (Los Gatos Research, Mountain View, USA) operationally measures CO_2 mixing ratios. This height is appropriate to precisely estimate CO_2 contents in the well-mixed PBL in the daytime (Haszpra *et al.*, 2015).

3. Verification of the model with observations

In this section, the performance of TerrSysMP-CO_2 is evaluated by comparing simulated meteorological conditions and atmospheric CO_2 variability with observations at the Jülich tower. Also, net ecosystem exchange (NEE) is compared with fluxes from EC stations. In order to capture diverse atmospheric states, we selected a period of eight consecutive days (3–10 June 2014) with different weather conditions. In the surroundings of the Jülich tower, more than 50% of the arable land is cultivated with cereal crops. With only one crop type (PFT = 15) in the current version of TerrSysMP-CO_2, plant physiological parameters of a cereal crop are most appropriate. Thus, we replaced the default plant physiological parameters of CLM for this PFT by the parameters of Sulis *et al.* (2015) adapted for extensively fertilized winter wheat in Central Europe.

3.1. *Meteorological situation*

We first describe the synoptic situation of this period. On 3 June, sunny phases alternated with showers in the afternoon. In the morning of 4 June ahead of a cold front, a band of light stratiform rain passed the domain followed by convective rain in the afternoon. On both days the temperatures were rather low and the wind continuously increased to a moderate breeze (Figure 5). The cold front passage in the late evening of 4 June induced intense showers together with a moderate to strong southwesterly wind which continued on 5 June. To the rear of the front, the weather was temporarily characterized by partial cloudiness and rather cool and dry air masses. In the following days (6–8 June), with a southerly flow very warm and moist air masses were advected causing significant increases of temperature and humidity. The sky was completely clear on 6 June, and fair weather conditions dominated on 7 and 8 June. At noon on 9 June, Jülich was influenced by clouds of a supercell storm and in the evening a very severe squall line passed NRW with damaging wind gusts. Both convective systems are not captured by the model, probably because the ICs underestimated the convective activity. Instead, at night strong showers were simulated in the western part of the domain. On 10 June, again fair weather conditions occurred with some light showers in the evening.

In order to understand the behaviour of simulated and observed CO_2 mixing ratios at the Jülich tower, we compared simulated meteorological variables with the corresponding measurements on the tower (Figure 5, Table 2).

The 2 m temperatures were simulated realistically (RMSE = 1.95 °C, R^2 = 0.88). The underestimated daytime temperatures on 8 June were caused by simulated advection of cool air masses from cloudy regions in the western part of the domain. On several nights the 2 m temperatures were overestimated, explaining the small warm bias. This is of particular

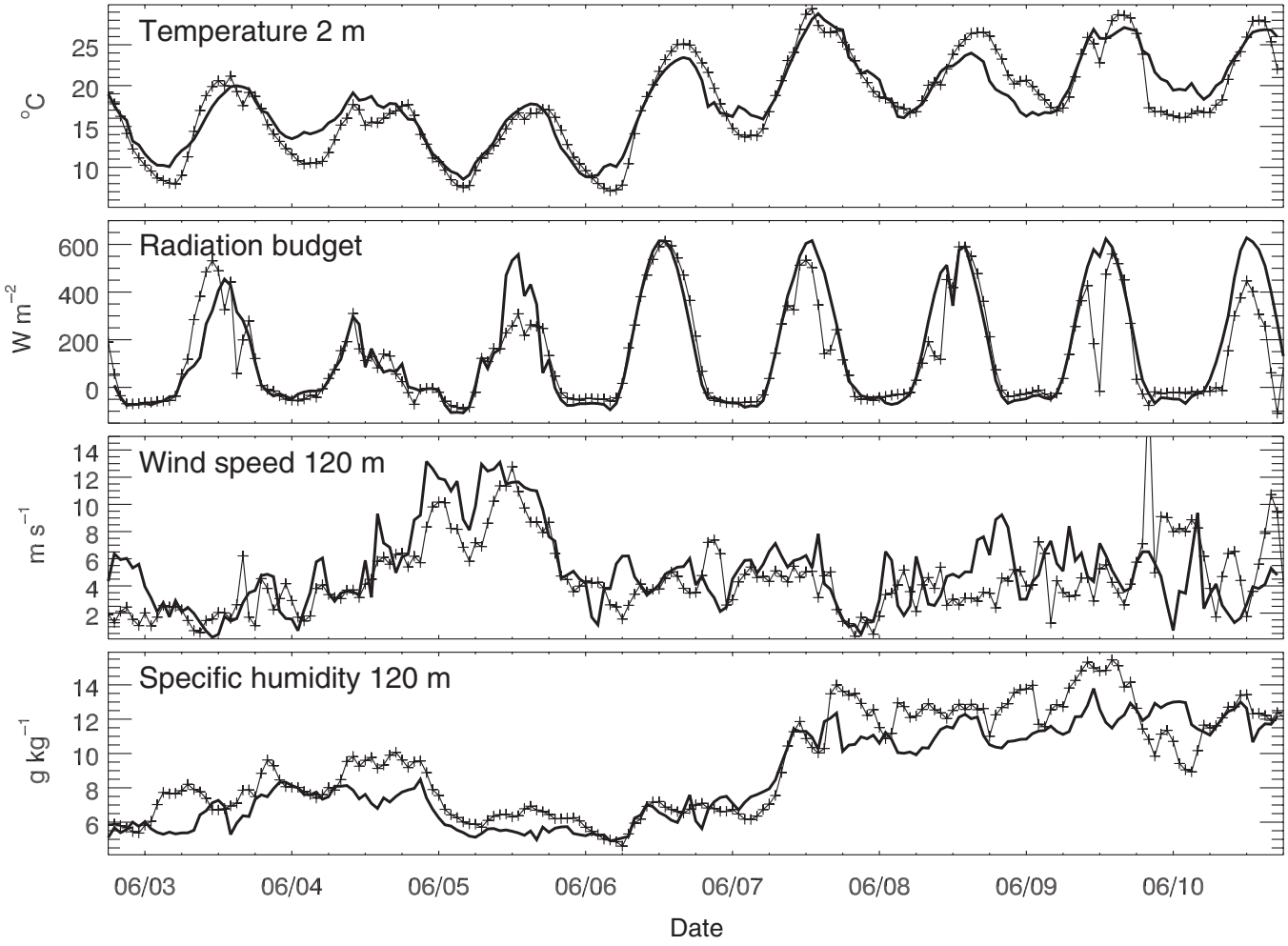

Figure 5. Comparison of simulated (thick solid lines) and observed (crosses) temperature (°C) at 2 m, total radiation budget (W m^{-2}), wind speed (m s^{-1}) and specific humidity (g kg^{-1}) at the Jülich tower between 3 and 10 June 2014.

Table 2. Statistical analysis of simulated against observed atmospheric variables at the Jülich tower between 03 and 10 June 2014: mean, root mean square error (RMSE), bias and correlation coefficient (R^2).

Variable	Mean	RMSE	Bias	R^2
Temperature 2 m (°C)	17.82	1.948	0.368	0.882
Temperature 120 m (°C)	18.82	1.869	−0.583	0.848
Radiation budget (W m^{-2})	124.1	108.4	25.36	0.701
Wind speed 120 m (m s^{-1})	4.620	1.427	0.501	0.580
Spec. hum. 120 m (g kg^{-1})	9.379	1.306	−0.765	0.787

importance in the following analysis (section 3.3). The simulated temperature values at 120 m agl were very similar to the observations (RMSE = 1.87 °C) but with a small cold bias.

The radiation budget was simulated fairly well (RMSE = 108 W m^{-2}; bias = 25.4 W m^{-2}; $R^2 = 0.70$). Even the radiation attenuation by cloudiness on 4 June was captured by the model. The only significant deviations from the measured radiation were underestimated cumulus clouds on 5 and 10 June.

The wind speed at 120 m agl agreed rather well with the observations (RMSE = 1.43 m s^{-1}; $R^2 = 0.58$). Even brief effects (e.g. windless conditions in the evening of 7 June) are simulated. In order to evaluate whether the synoptic flow was simulated realistically, a 6 h moving average was applied in the statistical analysis to filter out the strong fluctuations of the wind speed. The small bias of 0.5 m s^{-1} can be explained by a reduction of the observed wind speed caused by the forest surrounding the tower.

The specific humidity was rather well predicted (RMSE = 1.31 g kg^{-1}; bias = −0.77 g kg^{-1}; $R^2 = 0.79$), but with a small negative bias, especially on 8 and 9 June. This is possibly one of the reasons for the missing convective activity on 9 June.

Finally, it should be mentioned that this analysis is strongly affected by the missing squall line which caused significant deviations from the observations on 10 June. Almost all statistical scores are improved by excluding the last 24 h from the calculations. In particular, solar radiation is improved (RMSE = 99 W m^{-2}; bias = 14.4 W m^{-2}; $R^2 = 0.76$) but also the RMSE of wind speed (1.11 m s^{-1}) and temperature (2 m: 1.80 °C; 120 m: 1.62 °C) are distinctly lower for the first 7 days of the simulation. The rather low correlation of the wind speed (Table 2) results from the missing heavy gust front of the squall line whereas without the last 24 h the correlation is significantly better ($R^2 = 0.73$).

In general, the meteorological conditions at the Jülich tower are well represented by TerrSysMP-CO_2. An additional comparison with observations at DWD operational synoptic stations in other regions within the domain confirms that TerrSysMP-CO_2 simulates the synoptic situation realistically with deviations similar to the Jülich tower (not shown).

3.2. *Verification of simulated NEE*

The simulated NEE of different PFTs is compared with EC fluxes (Figure 6). For needleleaf trees, NEE is compared with fluxes above a spruce forest near Wüstebach. The simulated and observed CO_2 fluxes show a good agreement (RMSE = 5.63 μ mol(CO_2) m^{-2} s^{-1}; bias 1.05 μ mol(CO_2) m^{-2} s^{-1}). This holds in particular for 3 June and for 7–10 June. Hence, the plant physiological parameters seem to be appropriate for a typical needleleaf forest in Central Europe. Only on 5 June the measured

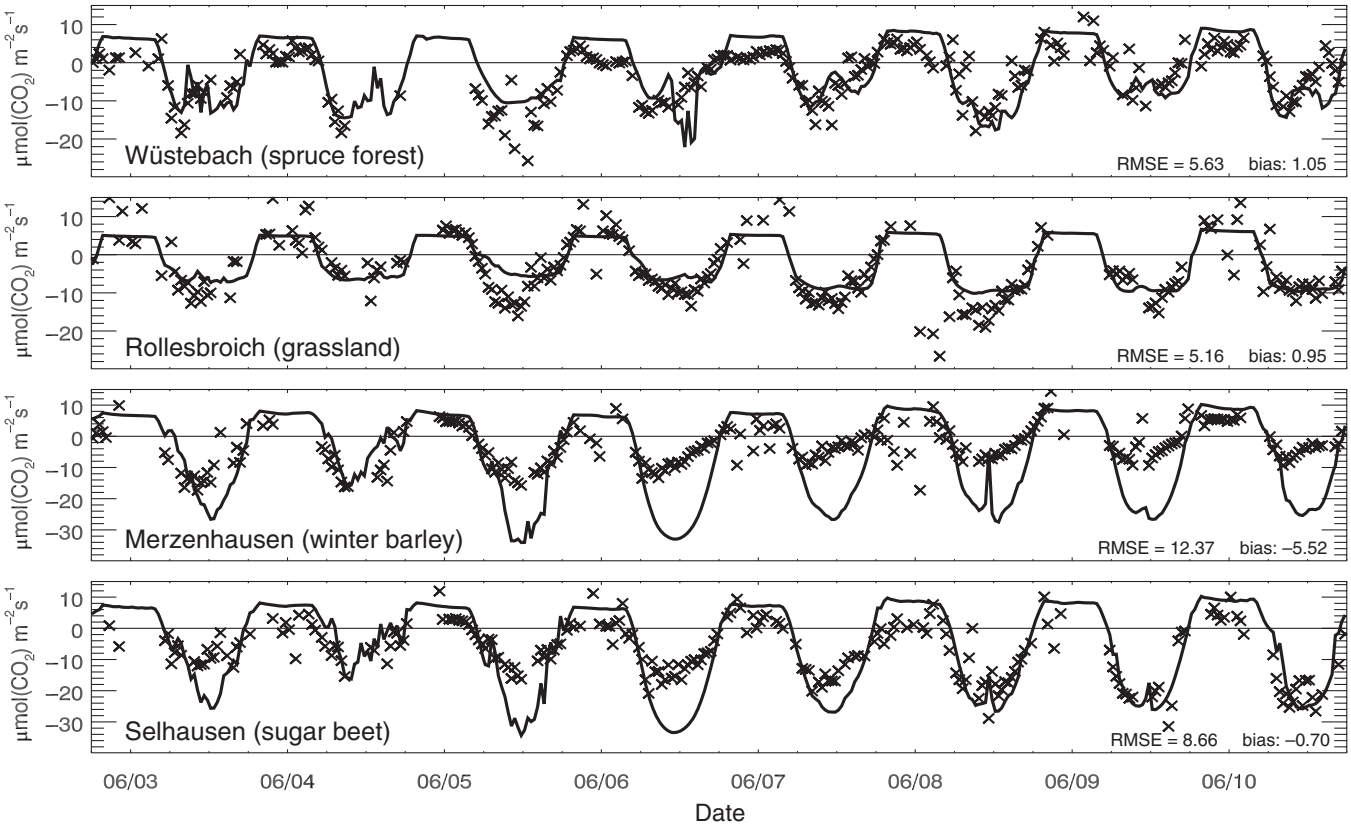

Figure 6. Comparison of simulated (solid lines) and observed (crosses) NEE (μ mol(CO_2) m^{-2} s^{-1}) at EC stations in Wüstebach, Rollesbroich, Merzenhausen and Selhausen between 3 and 10 June 2014.

CO_2 fluxes tended to be more negative than in the simulation, but high wind speeds on this day led to highly fluctuating (and possibly erroneous) EC fluxes. The small positive bias mainly results from too low *measured* nocturnal CO_2 release rates due to accumulation below the measurement height (40 m).

Similarly, the simulated daytime NEE is in accordance to observed CO_2 fluxes at the meadow near Rollesbroich (RMSE = 5.16 μ mol(CO_2) m^{-2} s^{-1}; bias 0.95 μ mol(CO_2) m^{-2} s^{-1}) which has a measured grass height of about 25 cm. On most days, the measured CO_2 uptake is in the range of the simulated NEE or slightly stronger. Nighttime respiration cannot be analyzed due to a lack of reliable EC fluxes.

In 2014, the Merzenhausen field was cultivated with winter barley. In contrast to forest and grassland, the measured NEE is not captured by the model (RMSE = 12.37 μ mol(CO_2) m^{-2} s^{-1}; bias -5.52 μ mol(CO_2) m^{-2} s^{-1}), simulating a much stronger CO_2 uptake in the daytime than observed. A closer look indicates that the measured CO_2 uptake decreased to the end of the period. The deviations have two reasons. First, winter barley has a phenological cycle earlier by several weeks than the mean cycle of (cereal) crops assumed by the model. Second, in this particular year, unusually high temperatures in spring induced the timing of phenological stages earlier than usual by about 10 days. Both effects cause a shift in the phenological stage of the Merzenhausen field compared to TerrSysMP-CO_2 using a 10 year mean for the seasonal course of LAIs for all crops in this region. Hence, in contrast to the model, barley fields in the flat terrain around Jülich already approached senescence, explaining both the observed decreasing daytime NEE and the overestimation of simulated NEE. A comparison of simulated NEE with a winter wheat (or rye) field, which is less senescent than barley, would probably lead to a much better agreement (Figure 11). Unfortunately, measurements for winter wheat are not available in 2014. Due to the earlier senescence of all cereal crops in 2014, the simulated daytime NEE seems to be slightly overestimated. Considering the high fraction of arable land in the flat terrain, this leads to lower CO_2 contents within the PBL than in reality (see next section).

The Selhausen site was cropped with sugar beet. Even utilizing cereal crop parameters, NEE agrees better than at the barley field (RMSE = 8.66 μ mol(CO_2) m^{-2} s^{-1}; bias -0.70 μ mol(CO_2) m^{-2} s^{-1}). The observed CO_2 uptake increased from 3 to 10 June due to rapidly growing plants. Between 27 May and 11 June, the vegetation height increased from 20 to 35 cm. On 8–10 June the simulated fluxes coincide well with the EC fluxes, whereas especially on 6 June the simulation overestimates the CO_2 uptake in the afternoon. The wilting of sugar beet is more sensitive to low soil moisture and low atmospheric humidity than is estimated with the cereal crop parameters (i.e. higher r_{st} than simulated), which explains the deviations on this day.

The model efficiency, expressed by R^2, is reasonable for the Wüstebach forest and for grassland (Rollesbroich) but seems to be weak for agriculture (not shown). In particular, the barley field (Merzenhausen) was not representative for cereal crops within the domain due to being on average several weeks later in senescence. Moreover, the statistical analysis is based on strongly fluctuating half-hourly EC fluxes (Figure 6), which explains the lower R^2 for canopy fluxes than for atmospheric state variables because these short-time fluctuations cannot be simulated. For a reliable estimation of the model performance, a statistical analysis of mean diurnal NEE cycles over a much longer time period and for several representative plants would be necessary.

3.3. CO_2 mixing ratios and PBL conditions

Diurnal CO_2 variations are height-dependent and strongly differ from day to day. Figure 7 depicts simulated and measured CO_2 mixing ratios at the Jülich tower for 3–10 June 2014. Measured CO_2 concentrations showed high diurnal variations on 3, 4, 7 and 8 June, but lower variations on the other days (Figure 7(a)). During the night, the highest CO_2 contents occurred at 12.5 m agl whereas the nocturnal increase became

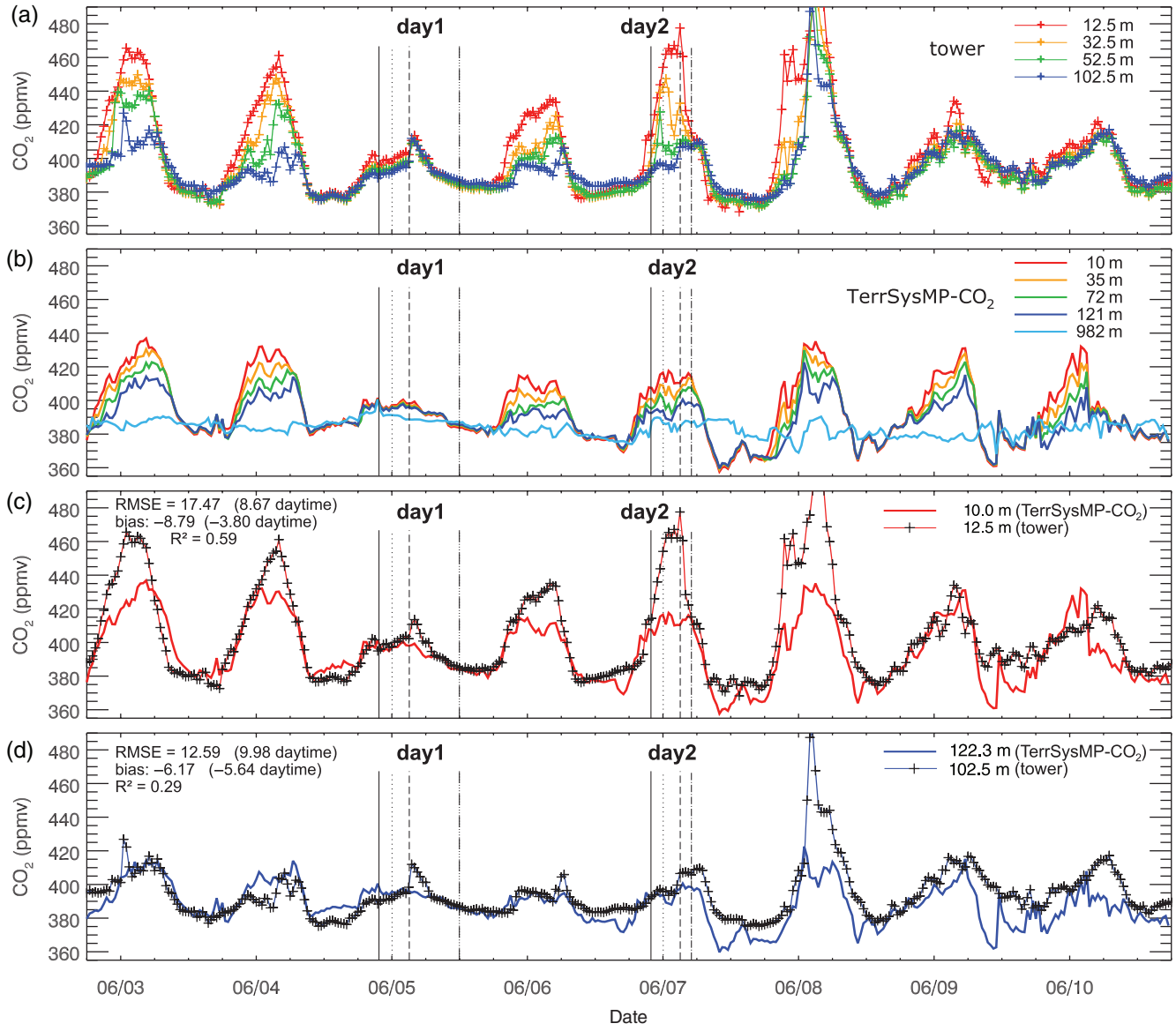

Figure 7. Diurnal variation of CO_2 mixing ratios (ppmv) at the Jülich tower: (a) measurements at several heights, (b) simulated by TerrSysMP-CO_2, (c) comparison of simulated (at 10 m agl) and observed (at 12.5 m agl), and (d) comparison of simulated (at 121 m agl) and observed (at 102.5 m agl). The vertical lines indicate the times of the profiles of 'day 1' and 'day 2', depicted in Figure 9.

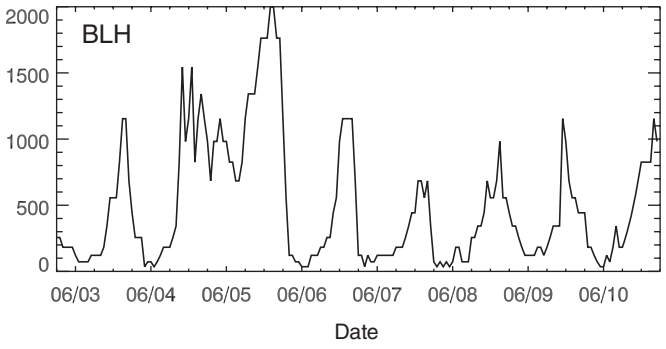

Figure 8. Diurnal variation of BLH (m) at the Jülich tower derived from TerrSysMP-CO_2 model output.

significantly lower at higher altitudes. In the daytime, CO_2 mixing ratios at all measurement heights were similar (due to a well-mixed PBL). At night on 5, 9 and 10 June, similar CO_2 contents were measured at all altitudes but with slightly stronger fluctuations at 12.5 m on 9 June. Two days ('day 1' and 'day 2') with contrasting behaviour at night are analyzed in more detail below.

The simulated CO_2 contents at the lower four model levels and at 982 m are shown in Figure 7(b). TerrSysMP-CO_2 captures the decreasing CO_2 amplitudes with height, however the vertical CO_2 gradients partially differ from the measurements. As in the observations, for 5 June the daily amplitude is lowest and almost not height-dependent. The simulated boundary layer height (BLH), calculated with the bulk Richardson number approach (Seibert *et al.*, 2000) using a critical value of 0.25, indicates that a shallow thermally stable PBL does not evolve during this night (Figure 8). Instead, strong winds to the rear of a cold front (Figure 5) cause efficient and deep turbulent mixing. On 5, 9 and 10 June the daily amplitudes are simulated faily well whereas on 3, 4 and 6–8 June the nocturnal CO_2 increase near the surface is underestimated by about 1/3 (Figure 7(c)). On these nights, shallow nocturnal PBLs formed (BLH < 100 m) characterized by weak winds and a very stable thermal stratification. The latter is partially underestimated by the model, which explains the deviations (see below). The only exception is the night of 10 June (after the missing squall line), showing again a stable thermal stratification (low BLH) resulting in overestimated vertical CO_2 gradients. With increasing BLH every morning vertical gradients of simulated and observed CO_2 mixing ratios diminish. The CO_2 contents about 1 km agl are decoupled from

the diurnal variations below, except for some short periods in the afternoon when the BLH exceeds this height level.

Figure 7(c) compares the simulated and observed CO_2 mixing ratios near the surface. The 12.5 m platform of the Jülich tower can be considered to be within the forest canopy. The above-described underestimated CO_2 mixing ratios on some nights are apparent. However, except for 7 and 9 June, the simulated daytime CO_2 contents agree well with the observations. Thus, both the model bias of −3.80 ppmv and the RMSE (8.67 ppmv), calculated for 0800–1930 UTC (i.e. convective PBL in the daytime), are considerably lower than the bias of −8.79 ppmv and the RMSE (17.5 ppmv) over the complete simulation period.

With increasing altitude, the differences decrease between simulated and observed nocturnal CO_2 contents. Similarly, in Sarrat *et al.* (2009) CO_2 contents at 60 m agl have been simulated better than at 20 m height. Compared to the surface level, at 121 m height the simulated CO_2 mixing ratios as well as the diurnal amplitudes agree better with the corresponding measurements (RMSE = 12.6 ppmv; bias −6.17 ppmv; Figure 7(d)). Relative to lower levels, the diurnal variation was considerably lower explaining the lower R^2 than at 10 m. The only exception is the night of 8 June showing very high CO_2 contents at all levels at the Jülich tower not occurring in the simulations. For about 2 h, at the tower the wind turned to SSW. Hence, advection of high CO_2 mixing ratios originating from a big coal-fired power plant at 10 km distance disturbs the observations. This temporary wind shift is not simulated, i.e. the CO_2 plume is not captured. This short period (8 June, 0000–0530 UTC) slightly distorts the statistical scores which are significantly better if this period is excluded from the statistical analysis (12.5 m: RMSE = 15.1 ppmv, bias −8.69 ppmv; 102.5 m: RMSE = 9.7 ppmv, bias −5.29 ppmv).

Especially in the daytime of 7 and 9 June, for several hours the simulated CO_2 contents are 10 ppmv (7 June) to 20 ppmv (9 June) lower than observed. On 7 June low simulated CO_2 mixing ratios originating over large arable areas are advected by a gentle to moderate southeasterly wind. As shown in the previous section, the simulated net CO_2 uptake of cereal crops is overestimated (e.g. bias of $-5.52\,\mu\,\mathrm{mol(CO_2)\,m^{-2}\,s^{-1}}$ for barley in Merzenhausen) causing CO_2 contents which are too low downstream of arable areas. Moreover, the BLH is rather low (< 500 m) in these periods. Similarly, on 9 June the negative deviations result from CO_2 advection from the same region but the simulated synoptic conditions (section 3.1) additionally affect the CO_2 contents, at least in the afternoon. Thus, horizontal advection strongly controls CO_2 mixing ratios measured on a tower in the daytime. This is in accordance to Tolk *et al.* (2009), who have found that strong CO_2 uptake of crops has a significant effect on CO_2 mixing ratios measured on the Cabauw tower which is located at a grassland site. At night, the Jülich tower is not significantly influenced by arable land in the surroundings because, in the stably stratified nocturnal PBL, locally respired CO_2 is more important than advective CO_2 transport (e.g. Oney *et al.*, 2015).

In order to better understand why the diurnal CO_2 variations are well simulated on some days but not on other days, vertical CO_2 profiles of two contrasting days are analyzed in combination with corresponding temperature profiles. 'Day 1' represents a positive example. On 4 June, between 2100 and 2300 UTC a cold front passed Jülich with enhanced wind speeds which continued over the following 18 h (Figure 5). Thus, free tropospheric CO_2 could be mixed to the surface explaining the low nocturnal CO_2 increase. The formation of a stable nocturnal PBL was inhibited resulting in similar CO_2 concentrations at all vertical levels (Figure 7). In the daytime, simulated and observed CO_2 mixing ratios continuously decrease and are in very good agreement.

At 2200 and 0000 UTC, the atmosphere is dry-adiabatically stratified (Figure 9(a)). In the well-mixed and deep PBL, a vertically homogeneous CO_2 distribution is simulated which is in accordance to the tower observations. At 0300 UTC, the simulated thermal stratification is no longer a dry adiabat. At the Jülich

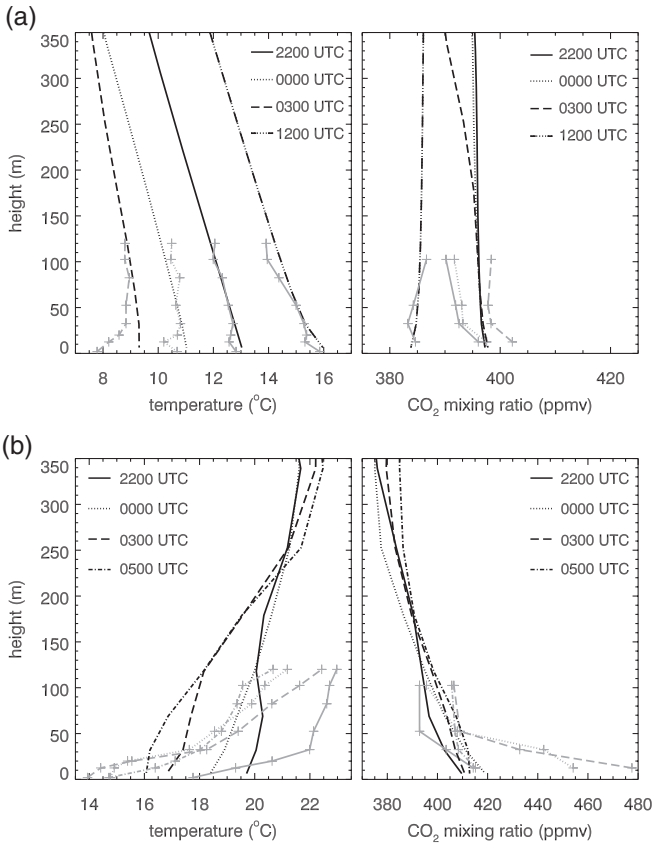

Figure 9. Vertical profiles of temperature (°C) and CO_2 mixing ratios (ppmv) at the Jülich tower at different times of (a) 'day 1' (2200 UTC on 4 June to 1200 UTC on 5 June 2014) and (b) 'day 2' (2200 UTC on 6 June to 0500 UTC on 7 June 2014). Black lines: simulated profiles, grey lines: observed profiles. The crosses indicate the heights of the tower observations.

tower almost isothermal conditions occurred above the forest top, with a weak inversion within the forest canopy. However, consistent with the simulations, a pronounced wind shear (12.5 m: 0.7 m s^{-1}; 120 m: 8.2 m s^{-1}) allowed efficient dynamically driven turbulent mixing, which also explaines the high BLH (Figure 8). At 1200 UTC, typical measured and simulated CO_2 and temperature profiles of a convective PBL can be seen.

In the night to 7 June ('day 2'), the differences in CO_2 increase at different heights of the tower were most pronounced. In contrast to 'day 1', the simulation strongly underestimates the nocturnal CO_2 contents at 12.5 m (and 32.5 m), whereas at the other levels the CO_2 mixing ratios are better in agreement (Figures 7(c) and (d)). The reasons for these deviations are analyzed in Figure 9(b).

At 2200 UTC, below 30 m a strong temperature inversion (4.2 °C increase with height) was observed whereas TerrSysMP-CO_2 simulates only a slight inversion (0.6 °C below 72 m). Thus, between 12.5 and 52.5 m the observed vertical CO_2 gradient was stronger than simulated. However, for this strong mismatch of the thermal stratification, even a stronger deviating vertical CO_2 gradient could be expected. A rather pronounced wind shear at the Jülich tower, not occurring in the simulation, inhibited a stronger near-surface CO_2 accumulation at this time. Until 0000 UTC, the observed temperature inversion (i.e. stable nocturnal PBL) extended to higher altitudes and the wind shear weakened. Hence, limited vertical turbulence caused an intense near-surface CO_2 accumulation as well as a strong vertical gradient between 12.5 and 52.5 m height. In contrast to the observations, a relatively uniform vertical temperature increase of only 2.8 °C is simulated below 250 m. Thus, the near-surface CO_2 mixing ratios and respective vertical gradients are significantly underestimated. Between 0000 and 0300 UTC the observed inversion further intensified to an exceptional degree (8.5 °C increase below 120 m) and was most pronounced around

the forest top (20.0–32.5 m). This explains the strong near-surface CO_2 accumulation as well as the distinctly lower concentrations at 32.5 and 52.5 m height. Again, the simulated PBL is deeper with strongly underestimated temperature inversion and vertical CO_2 gradients. Finally, at 0500 UTC the measured temperature inversion began to weaken and the wind had a distinct maximum at 82.5 m (not shown), both inducing stronger mixing. Thus, simulated and observed CO_2 profiles are in better agreement than in the previous hours.

This points out that, in situations with efficient turbulent mixing and high BLHs (e.g. 'day 1'), CO_2 mixing ratios and the rather homogeneous vertical CO_2 profiles are well simulated (cf. also 9 June). In contrast, the underestimated CO_2 mixing ratios near the surface result from a deficient representation of stable atmospheric stratifications causing a too strong turbulent vertical transport. This is a common problem of turbulence schemes used in NWP models (overestimating nocturnal BLHs combined with too weak inversions below), resulting in underestimated CO_2 accumulations near the surface (also found in Tolk *et al.*, 2009). The overestimated nocturnal 2 m temperatures (Figure 5) are a further indication of this problem. However, these mismatches are to some extent caused by the forest surrounding the small clearing where the Jülich tower is located. On clear-sky nights, the measured temperature and wind profiles regularly show a decoupling of the air within the canopy from the air above. This can be identified by almost calm conditions below 20 m reducing horizontal CO_2 transport as well as by a sharp temperature inversion between 20 and 32.5 m (e.g. 'day 2', 0000 and 0300 UTC) inhibiting the transport of CO_2 released by the canopy towards higher altitudes. These canopy effects cannot be considered by the current version of TerrSysMP-CO_2 using the roughness-length approach of a single vegetation surface. With consideration of drag effects, the influence of tall vegetation on the wind field could be accounted for (e.g. Dupont *et al.*, 2004; Aumond *et al.*, 2013).

4. Interaction with mesoscale meteorology

Canopy fluxes and the spatio-temporal variability of atmospheric CO_2 mixing ratios are analyzed for 26 May 2012. On this day the temperatures were moderate (≈ 20–$25\,^{\circ}C$ in the afternoon) and it was completely cloudless; this allowed a direct comparison of the simulated biosphere–atmosphere exchange of heat, water and CO_2 with observations without consideration of effects by clouds. The wind speeds decreased during the night whereas a moderate easterly wind (≈ 5–$8\,m\,s^{-1}$ at 10 m agl) occurred over the flat terrain between 1100 and 1400 UTC. Moreover, at this time in some areas the atmospheric humidity decreased considerably, leading to detrimental environmental conditions for plants.

Due to the predominant easterly flow over Central Europe the domain 'East' (Figure 4) was selected for the parent model assuming a background CO_2 content of 396 ppmv for IC and LBCs. The numerical simulation of the inner domain was initialized on 25 May 1800 UTC to be run for 30 h.

4.1. *Canopy fluxes and NEE*

The atmospheric CO_2 content in the PBL and the evolution of the convective PBL itself strongly depend on the canopy fluxes of CO_2, water and energy (Dolman *et al.*, 2006; Sarrat *et al.*, 2009; Tolk *et al.*, 2009). We performed two simulations, one with the default plant physiological parameters of CLM for *all* PFTs ('clmcrop'). Since the MODIS land cover data, used for the PFT classification (Figure 3(b)), assigns 81% of all arable land to cereal crops, in a second simulation ('cereal') we replaced the default crop parameters (PFT = 15) by the winter wheat parameters of Sulis *et al.* (2015), as also used in the simulations of section 3.

Figures 10(a)–(d) show NEE for both simulations. At night (0000 UTC) the vegetated canopy is a CO_2 source caused by soil and leaf respiration. In the 'clmcrop' simulation (Figure 10(a)) the fluxes are stronger for forests than for crops and grassland because (additionally to R_{auto} and R_{hetero}) the decomposition of above-ground litter and within the forest floor (R_O) contribute to the CO_2 flux. The highest respiration rates are simulated for broadleaf forests (8–$9\,\mu mol(CO_2)\,m^{-2}\,s^{-1}$); respiration of needleleaf forests is lower (6.5–$7.5\,\mu mol(CO_2)\,m^{-2}\,s^{-1}$). Due to stronger autotrophic respiration and considerably stronger leaf respiration of crops in the 'cereal' simulation, the contrast between forests and arable areas is less evident (Figure 10(b)).

With increasing photosynthesis in the early morning, the canopy becomes a net CO_2 sink. At noon (1200 UTC), in most regions the net CO_2 uptake (i.e. negative NEE) reaches its maximum. Figure 10(c) depicts NEE of the 'clmcrop' simulation. The strongest CO_2 uptake is simulated for broadleaf forests (11–$14\,\mu mol(CO_2)\,m^{-2}\,s^{-1}$), whereas the corresponding rates for grassland and crops are lower (6–$8\,\mu mol(CO_2)\,m^{-2}\,s^{-1}$). For crops these low values are surprising because measurements and several modelling studies in European regions (e.g. Ahmadov *et al.*, 2007; Sarrat *et al.*, 2009; Tolk *et al.*, 2009) indicate a much higher CO_2 uptake of cereal crops and vegetables. In contrast, in the 'cereal' simulation agricultural areas show by far the highest NEE (33–$38\,\mu mol(CO_2)\,m^{-2}\,s^{-1}$) caused by 2.5 to 3-fold higher photosynthesis rates (Figure 10(d)). Moreover, canopy transpiration of crops is 2.25 to 2.5-fold higher than in the 'clmcrop' simulation, leading to higher latent heat and lower sensible heat fluxes (not shown). The more efficient photosynthesis mainly results from improved parameters controlling RuBisCO enzyme kinematics (Sulis *et al.*, 2015, Table 1). For winter wheat, amongst others, a lower leaf C:N ratio of 14.0 ('clmcrop' 25.0) and a triplication of N in RuBisCO increases $V_{c,max}$ and thus photosynthesis. This is probably related to fertilization which is not accounted for in the 'clmcrop' parameters (Sulis *et al.*, 2015). Finally, a lower m in Eq. (1) allows for a higher photosynthesis rate for the same r_{st}.

Moreover, Figures 10(c) and (d) show rather low NEE rates of needleleaf forest in the central Eifel region (3–$6\,\mu mol(CO_2)\,m^{-2}\,s^{-1}$) being lower than in the late morning. This reduction is correlated with the above-described decrease of atmospheric humidity in this region (simulated dew point temperatures of 1–$3\,^{\circ}C$) in combination with increasing temperatures and wind speeds. An analysis of the simulated stomatal resistance (r_{st}) indicates values of about 600–$1200\,s\,m^{-1}$ in the entire domain, which is considerably higher than for optimum conditions ($r_{st} \approx 150\,s\,m^{-1}$). The highest resistances are simulated for needleleaf forests with 1800–$2100\,s\,m^{-1}$ (not shown). This means that on this particular day, due to limited soil moisture, the atmospheric conditions require a partial closure of leaf stomata at noon to avoid desiccation, to which needleleaf forests are most sensitive, consistent with the findings of Sarrat *et al.* (2009). Finally, we have to mention that for urban areas R_{hetero} is neglected and a low LAI of 0.6 only allows for weak fluxes of R_{auto}, R_L^{can} and A^{can}, i.e. weak NEE rates both at night and in the daytime.

Figures 10(e) and (f) show the variation of heterotrophic respiration in the mineral soil (R_{hetero}) and in the forest floor (R_O). The lowest rates are simulated at 0700 UTC with $1.6\,\mu mol(CO_2)\,m^{-2}\,s^{-1}$ for arable soils and 3.6–$4.6\,\mu mol(CO_2)\,m^{-2}\,s^{-1}$ in forests with the highest rates in the Rhine valley (Figure 10(e)). At 1500 UTC, heterotrophic respiration reaches its maximum (Figure 10(f)) with slightly higher values for arable soils and 4.4–$5.8\,\mu mol(CO_2)\,m^{-2}\,s^{-1}$ in forests, depending on topographic height. The rates of needleleaf and broadleaf forests are similar. The lower respiration rates of arable soils result from lower TOC contents in the entire soil column and from a negligible organic matter layer ($R_O = 0$ in TerrSysMP-CO_2). The stronger diurnal variation in forests than in agricultural regions can be explained by higher TOC contents in the topsoil where T_{soil} shows both a pronounced diurnal variation and higher values than in the subsoil in the afternoon. Moreover,

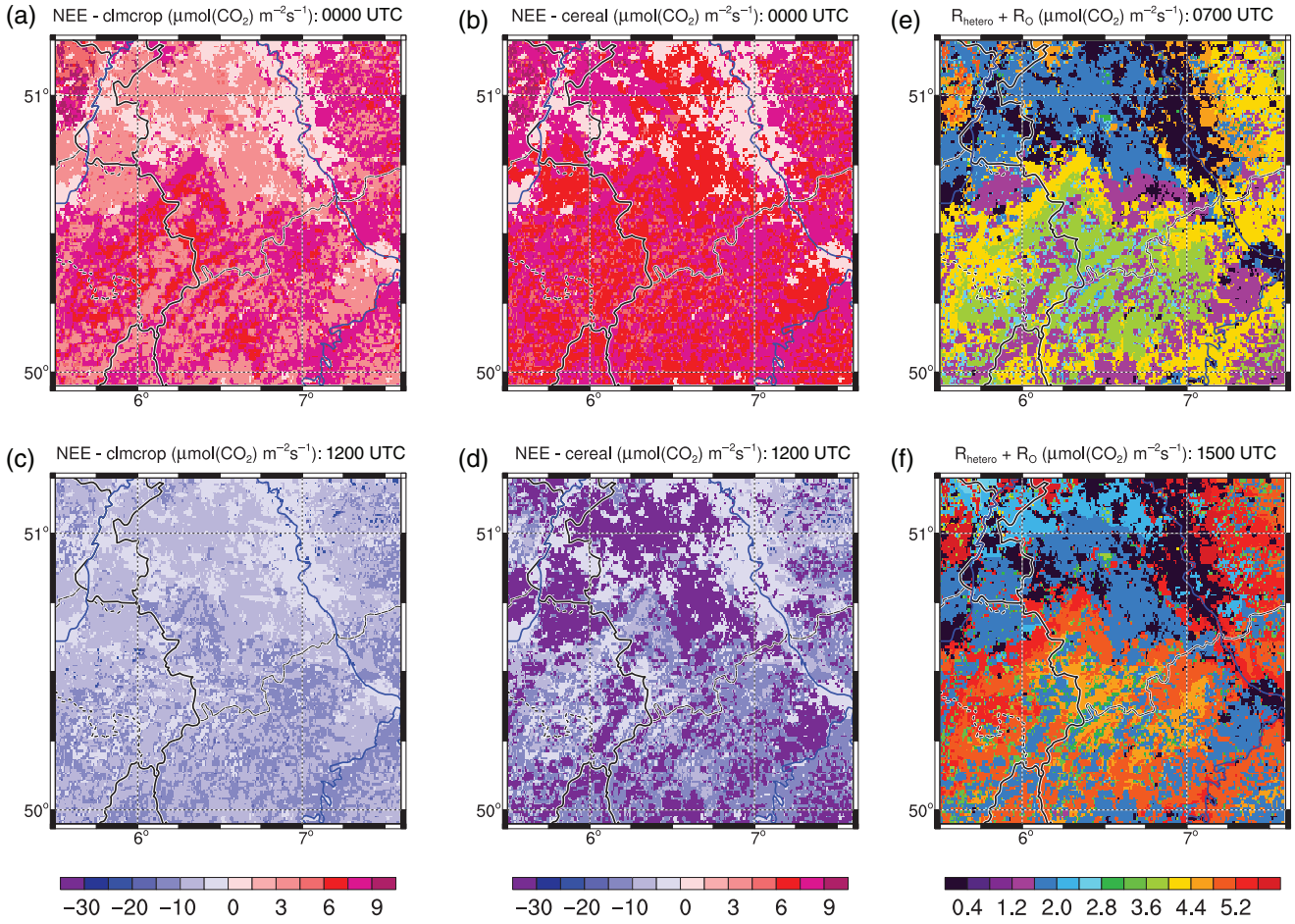

Figure 10. Simulated NEE (µ mol(CO_2) m^{-2} s^{-1}) on 26 May 2012 at (a, b) 0000 UTC and (c, d) 1200 UTC for the (a, c) 'clmcrop' and the (b, d) 'cereal' simulation. (e, f) show the total heterotrophic respiration ($R_{hetero} + R_O$) (µ mol(CO_2) m^{-2} s^{-1}) at (e) 0700 UTC and (f) 1500 UTC.

respiration of litter and respiration in the first few centimetres of soil (O horizon) are strongly temperature dependent and contribute significantly to soil respiration. Despite rather dry conditions prior to the simulation, soil moisture limitation is weak with a maximum reduction of about 10% in the lee of the Eifel. Hence, in the humid climate moisture reduction of soil respiration (Eq. (4)) in loamy soils is rather low, except after heavy rain events causing (super-)saturated soils (not shown).

As in section 3.2, the quality of simulated fluxes is evaluated with EC measurements of NEE, LH and SH fluxes at the crop site Merzenhausen (ME, winter wheat in 2012) and at the grassland sites Rollesbroich (RO) and Niederzier (NI) (Figure 11). For this day no data are available for the forest site Wüstebach.

Obviously, in the daytime the 'clmcrop' simulation (dashed lines in Figure 11) cannot capture the strong CO_2 uptake of winter wheat (Merzenhausen). This is consistent with a significant underestimation (overestimation) of LH (SH) fluxes. A possible reason of these deviations may be a too low LAI (2.2 in TerrSysMP-CO_2), compared to LAI measurements performed at this site and other cereal crop fields in this region. Moreover, the N limitation factor of 0.61 (i.e. 39% reduction to maximum photosynthesis) used for crops in CLM by default can be adapted for fertilized fields. However, the most important reason for the too weak CO_2 uptake is the inappropriate plant physiological parameter set of PFT = 15 in CLM. Noticeable in all simulated NEE curves of crops in this and other case-studies is a flattening between 0900 and 1700 UTC not occurring in the observations. Without any other restrictions, the crop parameters in the 'clmcrop' simulation lead to a $V_{c,max}$ of 20–25 µ mol(CO_2) m^{-2} s^{-1} for the simulated afternoon temperatures. Thus, the capacity utilization limitation (section 2.1.2) as upper limit of photosynthesis is already reached for leaf photosynthesis rates of 10–12.5 µ mol(CO_2) m^{-2} s^{-1}. In combination with respiration, this limitation explains the saturation of NEE at about −8 µ mol(CO_2) m^{-2} s^{-1}. In contrast, the winter wheat parameters of Sulis *et al.* (2015) ('cereal' simulation) clearly represent NEE and LH fluxes better (solid lines) due to a much higher $V_{c,max}$ (Table 1). SH fluxes are still slightly overestimated by the model. Finally, chamber measurements made on the previous day (25 May 2012) show that the simulated soil respiration agrees with observations at a further crop field (Selhausen; Figure 12).

CO_2 assimilation of the meadow in Rollesbroich between 0700 and 1600 UTC is underestimated. The saturation again indicates a capacity utilization limitation of simulated grassland at lower photosynthesis rates than for midlatitude meadows, but in contrast to agriculture, grassland clearly plays a minor role for this domain (5% land cover). Soil respiration is well estimated, proven by the agreement between simulated and measured NEE at night. Consistent with the underestimation of NEE, the simulated LH (SH) fluxes are too low (high). The measured daytime CO_2 fluxes at the meadow near Niederzier better coincide with the simulations. Thus, the partitioning of LH and SH is better than at Rollesbroich with only slightly lower (higher) simulated LH (SH) fluxes. One reason for the different measured fluxes of grassland is the lower canopy height (≈ 10 cm) in Niederzier compared to the two meadows influencing the EC fluxes in Rollesbroich (56 and 20 cm). The reduction of simulated NEE between 1100 and 1500 UTC is caused by a partly stomatal closure as response to low simulated dew-point temperatures and limited soil moisture in this region in the afternoon. A similar but weaker reduction can also be seen at Rollesbroich.

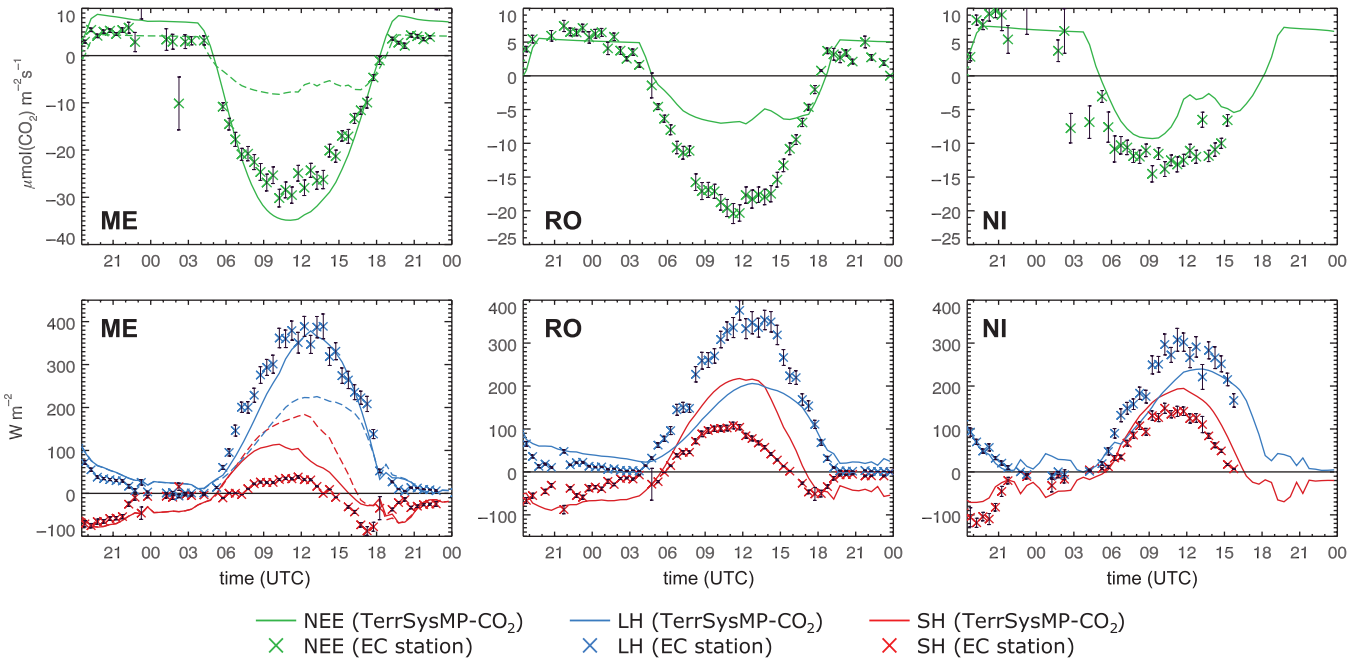

Figure 11. Comparison of simulated NEE (μ mol(CO_2) m^{-2} s^{-1}), LH and SH fluxes (W m^{-2}) with EC fluxes at Merzenhausen (ME, winter wheat), Rollesbroich (RO, grassland) and Niederzier (NI, grassland) between 1800 UTC on 25 May and 0000 UTC on 27 May 2012. At Merzenhausen the solid lines correspond to the 'cereal' simulation and the dashed lines to the 'clmcrop' simulation. The error bars denote the random errors of the measurements.

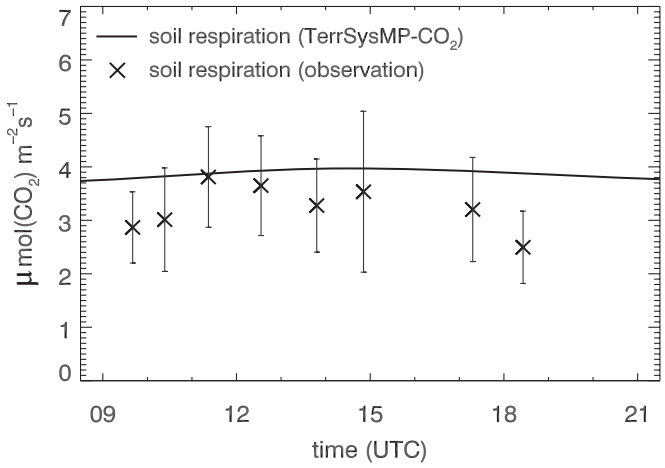

Figure 12. Comparison of simulated and observed total soil respiration (μ mol(CO_2) m^{-2} s^{-1}) at the Selhausen site (winter wheat) on 25 May 2012. The error bars denote the standard deviation of the measurements.

4.2. *Mesoscale atmospheric CO_2 distribution*

The relative influence of synoptic and mesoscale transport, diverse land cover and orography on the spatio-temporal variability of near-surface CO_2 mixing ratios is investigated over the rather complex and heterogeneous region described in section 2.2.1.

During the night, it is mainly respiration which causes a continuous increase of atmospheric CO_2 contents due to a low BLH. In the early morning (0400 UTC), the CO_2 mixing ratios are distributed very heterogeneously (Figure 13(a)). High CO_2 contents (420–440 ppmv) occur in the flat terrain as well as in the Moselle valley and some other narrow valleys in the Eifel (e.g. 6.3–6.5°E, 50.5–50.75°N). In contrast, on mountain ridges in the Eifel, the CO_2 concentrations increase only slightly (400–410 ppmv) although these areas are dominated by forests with intense respiration rates. The enhanced CO_2 mixing ratios in narrow valleys seem to be resolved only with the high horizontal resolution of TerrSysMP-CO_2 because small-scale mountain–valley effects are responsible for the horizontal CO_2 gradients. The highest CO_2 mixing ratios are simulated in the windward north of the Eifel (435–450 ppmv). In this region, the synoptic-scale easterly wind in the flat terrain is modified, resulting in a confluent flow (persisting over several hours) and a lowering of the BLH (not shown). This emphasises that in this case-study both the synoptic flow and mesoscale changes of the wind field, induced by orographic effects (e.g. windward of the Eifel, valley breeze), are mainly responsible for the CO_2 distribution in the early morning. The heterogeneous patterns of respiration due to different PFTs are less relevant.

With the onset of photosynthesis after sunrise (≈0400 UTC), in rural areas the CO_2 mixing ratios rapidly decrease within 2 h although the net CO_2 uptake is rather low in the early morning (Figure 13(b)). The transition from a shallow nocturnal PBL to a deep convective PBL occurs later in the morning than the change from a positive to a negative NEE, explaining the strong CO_2 decrease. In contrast, road traffic rapidly increases (morning rush hour at 0600–0700 UTC). Windless conditions (< 1 m s^{-1}) in the Rhine valley allow for local CO_2 accumulations around the cities of Bonn, Cologne and Dusseldorf. A similar effect can be seen for Liège. Compared to a simulation without anthropogenic emissions, the CO_2 mixing ratios in the flat terrain are about 5–10 ppmv higher with local deviations > 30 ppmv in urban regions along the river Rhine (not shown). Due to the contrasting behavior of rural and urban areas, at 0600 UTC the greatest heterogeneity is simulated with about 395 ppmv in eastern Belgium and northeast of Cologne and more than 440 ppmv in the metropolitan areas. The local effects of fossil fuel emissions in cities have been also shown (e.g. in Pérez-Landa *et al.*, 2007), but with a very simplified representation of anthropogenic emissions in their study.

Between 0700 and 1200 UTC, in most regions CO_2 continuously decreases to 385–395 ppmv (i.e. below the background CO_2 content). In the flat terrain west of the Rhine, at 0900 UTC (Figure 13(c)) downstream of urban areas and big power plants the CO_2 mixing ratios are still about 3–10 ppmv higher (395–410 ppmv) than without fossil fuel emissions; a rather low BLH (400–500 m) also contributes to this. In general, with growing BLH the horizontal CO_2 gradients begin to diminish. Compared to the morning hours, at 1600 UTC (Figure 13(d)) the CO_2 distribution is less heterogeneous (380–395 ppmv) which is the result of a moderate synoptic flow in combination with turbulent vertical mixing within the 1300–2000 m deep

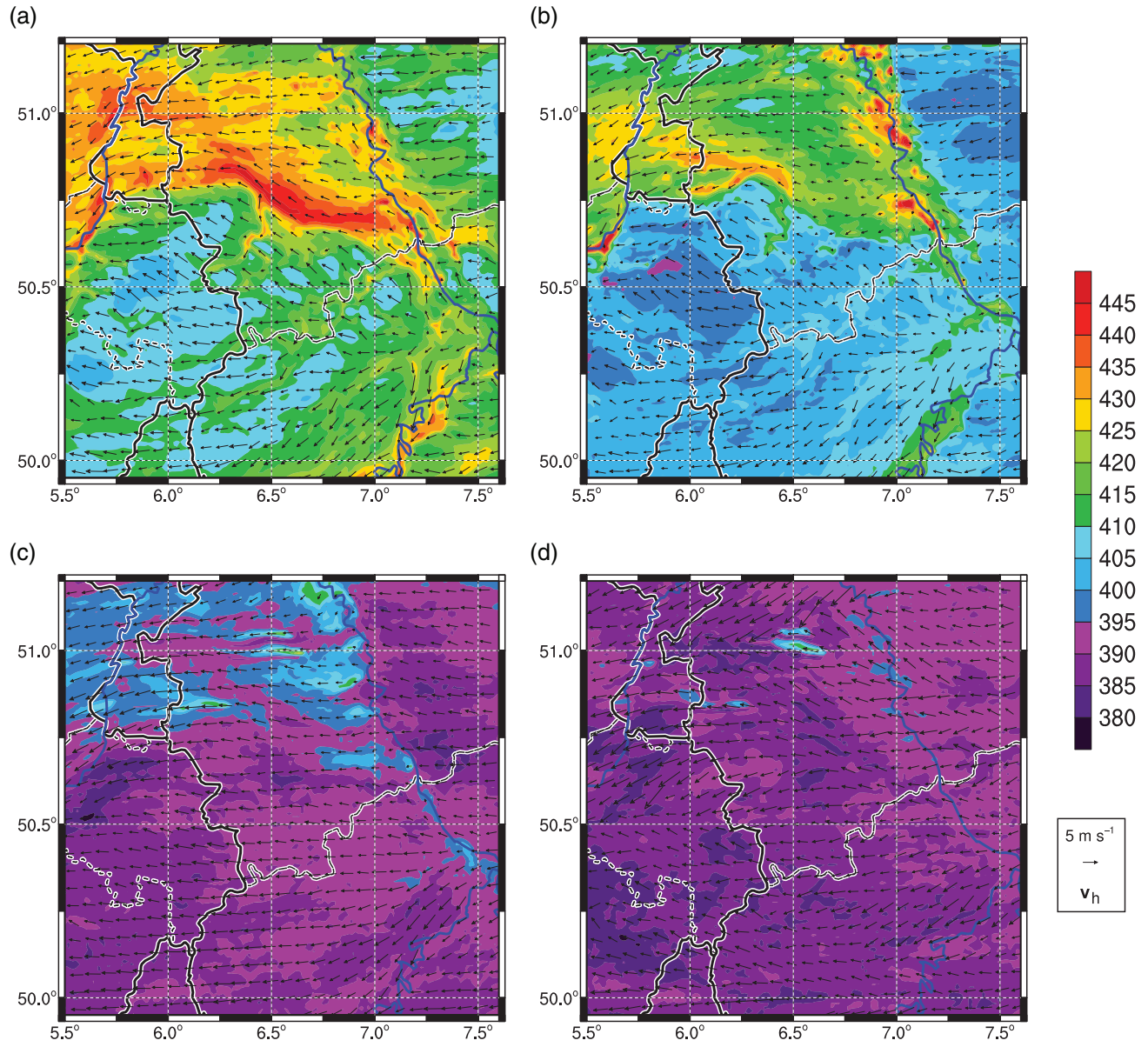

Figure 13. Simulated CO_2 mixing ratios (ppmv, shading) and horizontal wind ($m\,s^{-1}$, arrows) at the lowest COSMO level (≈ 10 m agl) on 26 May 2012 ('cereal' simulation): (a) 0400 UTC, (b) 0600 UTC, (c) 0900 UTC, (d) 1600 UTC.

convective PBL. Vertical cross-sections indicate almost constant CO_2 mixing ratios below the BLH (not shown).

In the afternoon, the CO_2 concentrations within the PBL are below the background CO_2 content which remains rather constant in the free atmosphere. Thus, on this clear-sky day, the land surface is a sink of atmospheric CO_2. Table 3 lists the contributions of the surface CO_2 budget averaged over the entire model domain from 25 May 1800 UTC to 26 May 1800 UTC. It indicates a biogenic sink of $-4.297\,\mu mol(CO_2)\,m^{-2}\,s^{-1}$ and a total sink (including anthropogenic emissions) of $-1.385\,\mu mol(CO_2)\,m^{-2}\,s^{-1}$. In the considered region, anthropogenic emissions are an intense CO_2 source (28% of total CO_2 source). The net surface CO_2 sink in the 'cereal' simulation seems to be more realistic than the gain ($+1.757\,\mu mol(CO_2)\,m^{-2}\,s^{-1}$) in the 'clmcrop' simulation. It is consistent with a measured CO_2 decrease at the Jülich tower in spring and summer (not shown) and with the maps of monthly CO_2 fluxes (CarbonTracker Europe, 2014).

Table 3. Surface CO_2 budget ($\mu mol(CO_2)\,m^{-2}\,s^{-1}$) of the 'cereal' and 'clmcrop' simulations.

Source/sink	Cereal	clmcrop
Photosynthesis	−11.735	−6.982
Leaf respiration	*1.568*	*0.524*
Soil respiration	*5.870*	*5.304*
Total respiration	7.438	5.827
Net biosphere budget	−4.297	−1.154
Anthropogenic emissions	2.912	2.912
Total budget	**−1.385**	**+1.757**

4.3. *Effect of modified canopy fluxes on PBL conditions*

As expected, the strong influence of different plant physiological parameters of crops (PFT = 15) on the canopy exchange of CO_2 (i.e. NEE), water and energy (LH and SH fluxes) has an effect on the atmospheric conditions within the PBL. Higher rates of above-ground and below-ground autotrophic respiration ($R_L^{can} + R_{auto}$) in the 'cereal' simulation during the night cause 5–15 ppmv higher near-surface CO_2 mixing ratios in the flat terrain where agriculture is the dominant land use (not shown). In contrast, in the daytime the stronger CO_2 uptake results in lower CO_2 mixing ratios near the surface. This means that a higher diurnal CO_2 variation is simulated in the 'cereal' simulation than in the 'clmcrop' simulation, combined with a faster CO_2 decrease

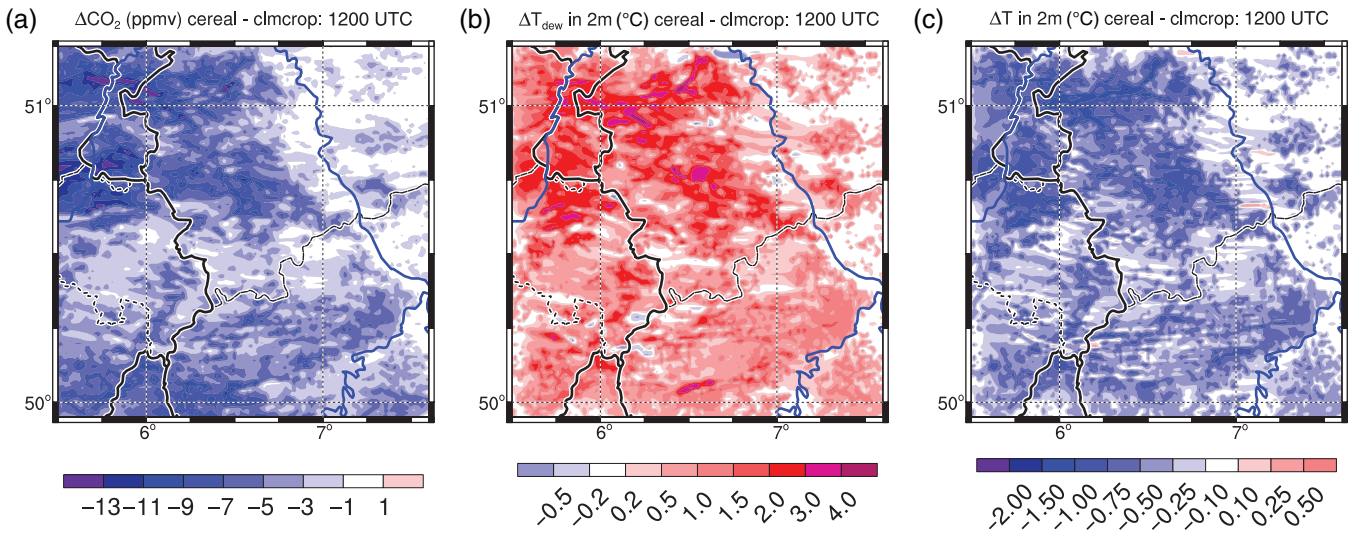

Figure 14. Differences 'cereal' minus 'clmcrop' simulations at 1200 UTC on 26 May 2012: (a) CO_2 mixing ratio (ppmv) at the lowest COSMO level (≈ 10 m agl), (b) 2 m dew point temperature (°C) and (c) 2 m temperature (°C).

in the morning. Figure 14(a) depicts the difference of the near-surface CO_2 mixing ratios of both simulations at 1200 UTC. Above and downstream of agricultural areas in the flat terrain west of the river Rhine, 5–10 ppmv (locally 15 ppmv) lower CO_2 mixing ratios are simulated in the 'cereal' simulation whereas, in the Bergisches Land east of the Rhine, the difference is less because forests dominate in and upstream of this region.

Distinctly higher transpiration rates in the 'cereal' simulation increase the humidity in the PBL. Figure 14(b) shows on average 1–2 °C (locally 4°C) higher 2 m T_{dew} at 1200 UTC. In contrast, the 2 m temperature is on average 0.5–0.75 °C (locally > 1°C) lower than in the 'clmcrop' simulation due to stronger evaporative cooling (Figure 14(c)). Vertical cross-sections indicate similar differences up to the BLH. Thus, the effects of CO_2, T_{dew} and T, depicted in Figure 14, are representative for the entire convective PBL.

5. Summary and conclusions

We have described and applied a new coupled biosphere–atmosphere model (TerrSysMP-CO_2) for the simulation of mesoscale and diurnal variations of atmospheric CO_2 mixing ratios in a region with heterogeneous land use, densely populated areas and complex terrain. The process-based canopy parametrization uses the prognostically varying atmospheric CO_2 contents at the surface to calculate canopy transpiration and photosynthesis. Moreover, the model includes an advanced representation of soil respiration, distinguishing between heterotrophic and autotrophic respiration and explicitly considering the effect of varying soil moisture. Another novel concept is the use of measured TOC profiles for the calculation of heterotrophic respiration. In the numerical simulations, the strong heterogeneity of the land surface is accounted for by using a fine horizontal grid resolution (500 m) for the land surface component, but also the atmospheric conditions are simulated with a fine grid spacing (≈ 1 km) to capture relevant mesoscale flow patterns. High-resolution anthropogenic emissions, separated into several emission classes, take into account the human-induced influence on the spatio-temporal CO_2 distribution within the PBL.

The model performance has been tested for eight consecutive days with different weather conditions. A comparison of temperature, radiation, wind and humidity with corresponding measurements on a meteorological tower shows high correlations with rather low biases. Thus, the synoptic situation of this period is captured by the model. A significant weakness is the slightly overestimated 2 m temperatures on cloudless nights caused by simulated turbulent mixing which is too strong. NEE (and energy fluxes) of needleleaf forests and grassland are simulated fairly well, but the model performance strongly depends on the grass height. For agriculture the evaluation is more difficult. With only one PFT used for the entire arable area, the *simulated* NEE at each agricultural grid point is *comparable*. In contrast, *real* NEE of arable land in this region is very *heterogeneously* dependent on the different physiological behaviour and phenological stages of different crops. Thus, the model fails to simulate NEE for a barley field in 2014 having a rather early phenological cycle. However, in the clear-sky case in 2012, the CO_2 uptake of winter wheat in the mature stage is well simulated. This shows that the physiological parameters are appropriate for cereal crops when the phenological stage coincides with the observed field. We conclude that only one PFT representing agriculture is insufficient for a region where very diverse crops (e.g. cereals, sugar beet, maize, vegetables) are cultivated. In a later version of TerrSysMP-CO_2, this variation will be considered by integrating additional agricultural PFTs. Finally, we want to mention that only a limited time period has been used for verification. For an extensive validation of the performance of the new model, longer periods and a comparison with several synoptic stations would be necessary.

Both CO_2 measurements on a meteorological tower and the simulations show very different nocturnal CO_2 increases, depending on height and on atmospheric conditions. In situations with efficient turbulent mixing (e.g. convective PBL in daytime, frontal passage with strong winds) the rather homogeneous vertical CO_2 profiles are well predicted. However, especially on cloudless nights with weak winds, the simulated near-surface CO_2 accumulation, vertical CO_2 gradients and vertical stability are underestimated on several days. We conclude that pronounced temperature inversions, i.e. very stably stratified nocturnal PBLs, are not sufficiently reproduced by the model, as supported by slightly overestimated 2 m temperatures on these nights. Thus, too efficient vertical CO_2 transport inhibits realistic CO_2 accumulations in the simulations. This is an important message for the meteorological community indicating that parametrization currently used in most NWP models show deficiencies in simulating the transport of CO_2 (or air pollutants) in such situations. However, we have to mention that some of these mismatches are also affected by the forest surrounding the tower. This often results in a decoupling of the air within the forest canopy from the air above; this cannot be addressed with a single vegetation surface in the model. In a future version of TerrSysMP-CO_2, the dynamical influence of tall vegetation will be accounted for by including drag terms in the dynamic equations.

The simulated exchange of water, heat and CO_2 between the canopy and the atmosphere has been analyzed for two different crop physiological parameter sets. Compared to EC fluxes on a winter wheat field on a clear-sky day, the simulation using the default parameters of CLM significantly underestimates the CO_2 uptake of cereal crops in the daytime. Similarly, canopy transpiration (and latent heat fluxes) are underestimated, resulting in too high sensible heat fluxes. In contrast, the simulation using plant physiological parameters calibrated for winter wheat in Central Europe indicate a much better agreement of NEE, latent and sensible heat fluxes to the observations. Adopted parameters controlling photosynthetic efficiency, being appropriate for fertilized cereal crops, explain this improvement. The modified canopy fluxes strongly influence the simulated atmospheric conditions showing lower CO_2 contents, higher humidity and lower temperature in the entire convective PBL above and downstream of large agricultural areas. This emphasises that realistic canopy fluxes are essential for an accurate simulation of the atmospheric conditions within the PBL.

Soil respiration is simulated realistically by the advanced parametrization in TerrSysMP-CO_2. Higher respiration rates and stronger temporal variations are simulated for forests than for arable soils. This is caused by higher TOC contents in total and especially in the topsoil (where distinct variations of T_{soil} occur) as well as by respiration of litter and within the forest floor which are highly sensitive to temperature changes.

The mesoscale application of the model shows no clear correlation between simulated CO_2 mixing ratios and the predominant land use. Hence, the convective boundary-layer budget method (Lloyd *et al.*, 2001), deriving NEE by means of CO_2 profiles in the well-mixed PBL at the landscape scale ($\approx 1-10$ km), cannot be applied in regions with complex terrain. Instead, distinctly higher near-surface CO_2 concentrations are simulated in valleys or to windward of the Eifel than above elevated mountain ridges. Thus, we conclude that in regions with hilly terrain, the CO_2 patterns are strongly influenced by terrain-induced local circulations, especially at night and in the morning. In the afternoon, efficient turbulent mixing and a high BLH significantly reduce horizontal CO_2 gradients within the convective PBL. In a supplementary study, TerrSysMP-CO_2 will be used to investigate in detail the influence of complex terrain on the thermodynamic behaviour of the atmosphere controlling the near-surface CO_2 distribution. Additionally, the appropriate grid resolution necessary to resolve these processes will be investigated. This is a very important question for the use of CO_2 concentrations from continental measurement sites in regional-scale inverse modelling. Regional models using grid sizes of several kilometres may be insufficient to realistically simulate the spatial CO_2 distribution in regions with complex terrain. This may be one reason for the mismatch between local flux measurements and CO_2 fluxes estimated from inverse modelling. Thus, TerrSysMP-CO_2 provides important information to close the gap between these scales. Moreover, significantly higher CO_2 contents are simulated in and around big cities, indicating intense CO_2 sources from fossil fuel emissions from industrial or urban regions. The very-high-resolution emission dataset used in the TerrSysMP-CO_2 simulations will allow us to quantify the anthropogenic effect for different weather situations in a future study.

Acknowledgements

We gratefully acknowledge financial support from SFB/TR32 'Patterns in Soil–Vegetation–Atmosphere Systems: Monitoring, Modelling and Data Assimilation' (TRR 32/3 2015), funded by the German Science Foundation (DFG). We also thank the German Meteorological Service (Deutscher Wetterdienst) for providing the COSMO model and the analysis data needed for driving the model. Moreover, we thank A. Graf from the Forschungszentrum Jülich GmbH, IBG-3, for the technical support with the CO_2 mixing ratio measurements and for providing the EC data, and M. von Hobe from the Forschungszentrum Jülich GmbH, IEK-7, for providing additional CO_2 measurements on the Jülich tower. We also acknowledge H. Denier van der Gon from the TNO for providing a preliminary version of the TNO-CAMS CO_2 emission inventory. Finally, we thank the two anonymous reviewers for their constructive suggestions which clearly improved the manuscript.

References

Ahmadov R, Gerbig C, Kretschmer R, Koerner S, Neininger B, Dolman AJ, Sarrat C. 2007. Mesoscale covariance of transport and CO2 fluxes: Evidence from observations and simulations using the WRF-VPRM coupled atmosphere-biosphere model. *J. Geophys. Res.* **112**: D22107. https://doi.org/10.1029/2007JD008552.

Aumond P, Masson V, Lac C, Gauvreau B, Dupont S, Berengier M. 2013. Including the drag effects of canopies: Real case large-eddy simulation studies. *Boundary-Layer Meteorol.* **146**: 65–80.

Baldauf M, Seifert A, Förstner J, Majewski D, Raschendorfer M, Reinhardt T. 2011. Operational convective-scale numerical weather prediction with the COSMO model: Description and sensitivities. *Mon. Weather Rev.* **139**: 3887–3905.

Bott A. 1989. A positive definite advection scheme obtained by nonlinear renormalization of the advective fluxes. *Mon. Weather Rev.* **117**: 1006–1016.

CarbonTracker Europe. 2014. 'Global monthly $1^\circ \times 1^\circ$ resolution CO2 flux data (2001–2011)'. ftp://ftp.wur.nl/carbontracker/data/fluxes/data_flux1x1_monthly (accessed 18 April 2017).

Coleman K, Jenkinson D. 2005. *RothC-26.3. A Model for the Turnover of Carbon in Soil, Model Description and Windows Users Guide*. IACR-Rothamsted: Harpenden, UK.

Collatz GJ, Ball JT, Grivet C, Berry JA. 1991. Physiological and environmental regulation of stomatal conductance, photosynthesis and transpiration: A model that includes a laminar boundary layer. *Agric. For. Meteorol.* **54**: 107–136.

Dai Y, Zeng X, Dickinson RE, Baker I, Bonan GB, Bosilovich MG, Denning AS, Dirmeyer PA, Houser PR, Niu G, Oleson KW, Schlosser CA, Yang ZL. 2003. The common land model. *Bull. Am. Meteorol. Soc.* **84**: 1013–1023.

Davin E, Seneviratne S. 2012. Role of land surface processes and diffuse/direct radiation partitioning in simulating the European climate. *Biogeosciences* **9**: 1695–1707.

Davin E, Stöckli R, Jaeger E, Levis S, Seneviratne S. 2011. COSMO-CLM2: A new version of the COSMO-CLM model coupled to the community land model. *Clim. Dyn.* **37**: 1889–1907.

Dolman A, Noilhan J, Durand P, Sarrat C, Brut A, Piguet B, Butet A, Jarosz N, Brunet Y, Loustau D, Lamaud E, Tolk L, Ronda R, Miglietta F, Gioli B, Magliulo V, Esposito M, Gerbig C, Korner S, Glademard O, Ramonet M, Ciasis P, Neininger B, Hutjes R, Elbers J, Macatangay R, Schrems O, Perez-Landa G, Sanz M, Scholz Y, Facon G, Ceschia E, Beziat P. 2006. The CarboEurope regional experiment strategy. *Bull. Am. Meteorol. Soc.* **87**: 1367–1379.

Dupont S, Otte T, Ching J. 2004. Simulation of meteorological fields within and above urban and rural canopies with a mesoscale model. *Boundary-Layer Meteorol.* **113**: 111–158.

FAO-UNESCO. 1975. *Soil Map of the World*, Volume V Europe. FAO, UNESCO: Rome.

Farquhar GD, von Caemmerer S, Berry JA. 1980. A biochemical model of photosynthetic CO2 assimilation in leaves of C3 species. *Planta* **149**: 78–90.

Gerbig C, Dolman AJ, Heimann M. 2009. On observational and modelling strategies targeted at regional carbon exchange over continents. *Biogeosciences* **6**: 1949–1959.

Haszpra L, Barcza Z, Haszpra T, Pátkai ZS, Davis KJ. 2015. How well do tall-tower measurements characterize the CO2 mole fraction distribution in the planetary boundary layer? *Atmos. Meas. Tech.* **8**: 1657–1671.

Jones C, McConnell C, Coleman K, Cox P, Falloon P, Jenkinson D, Powlson D. 2005. Global climate change and soil carbon stocks; predictions from two contrasting models for the turnover of organic carbon in soil. *Global Change Biol.* **11**: 154–166.

Kuell V, Bott A. 2008. A hybrid convection scheme for use in non-hydrostatic numerical weather prediction models. *Meteorol. Z.* **17**: 775–783.

Kuell V, Bott A. 2011. Simulation of non-local effects of convection with the hybrid mass flux convection scheme HYMACS. *Meteorol. Z.* **20**: 227–241.

Kuenen JJP, Visschedijk AJH, Jozwicka M, Denier van der Gon H. 2014. TNO-MACC_II emission inventory; a multi-year (2003–2009) consistent high-resolution European emission inventory for air quality modelling. *Atmos. Chem. Phys.* **14**: 10963–10976.

LANUV. 2012. *Fachinformationssystem Stoffliche Bodenbelastung*. Landesamt für Natur, Umwelt und Verbraucherschutz Nordrhein-Westfalen (LANUV): Recklinghausen, Germany.

Lloyd J, Taylor JA. 1994. On the temperature dependence of soil respiration. *Funct. Ecol.* **8**: 315–323.

Lloyd J, Francey RJ, Mollicone D, Raupach MR, Sogachev A, Arneth A, Byers JN, Kelliher FM, Rebmann C, Valentini R, Wong SC, Bauer G, Schulze ED. 2001. Vertical profiles, boundary layer budgets, and regional flux estimates for CO2 and its 13C/12C ratio and for water vapor above a forest/bog mosaic in central Siberia. *Global Biogeochem. Cycles* **15**: 267–284.

Mauder M, Cuntz M, Drüe C, Graf A, Rebmann C, Schmid HP, Schmidt M, Steinbrecher R. 2013. A strategy for quality and uncertainty assessment of long-term eddy-covariance measurements. *Agric. For. Meteorol.* **169**: 122–135.

Mellor GL, Yamada T. 1982. Development of a turbulence closure model for geophysical fluid problems. *Rev. Geophys. Space Phys.* **20**: 851–875.

Nicholls ME, Denning AS, Prihodko L, Vidale PL, Baker I, Davis K, Bakwin P. 2004. A multiple-scale simulation of variations in atmospheric carbon dioxide using a coupled biosphere–atmospheric model. *J. Geophys. Res.* **109**: D18117. https://doi.org/10.1029/2003JD004482.

Oleson KW, Lawrence DM, Bonan GB, Flanner MG, Kluzek E, Lawrence PJ, Levis S, Swenson SC, Thornton PE. 2010. 'Technical description of version 4.0 of the Community Land Model (CLM)'. NCAR/TN-478+STR, NCAR: Boulder, CO.

Oney B, Henne S, Gruber N, Leuenberger M, Bamberger I, Eugster W, Brunner D. 2015. The CarboCount CH sites: Characterization of a dense greenhouse gas observation network. *Atmos. Chem. Phys.* **15**: 11147–11164.

Pérez-Landa G, Ciais P, Gangoiti G, Palau JL, Carrara A, Gioli B, Miglietta F, Schumacher M, Millán MM, Sanz MJ. 2007. Mesoscale circulations over complex terrain in the Valencia coastal region, Spain –Part 2: Modeling CO2 transport using idealized surface fluxes. *Atmos. Chem. Phys.* **7**: 1851–1868.

Peters W, Krol MC, Van Der Werf GR, Houweling S, Jones CD, Hughes J, Schaefer K, Masarie KA, Jacobson AR, Miller JB, Cho CH, Ramonet M, Schmidt M, Ciattaglia L, Apadula F, Helta D, Meinhardt F, di Sarra AG, Piacentino S, Sferlazzo D, Aalto T, Hatakka J, Strom J, Haszpra L, Meijer HAJ, van der Laan S, Neubert REM, Jordan A, Rodo X, Morgui JA, Vermeulen AT, Popa E, Rozanski K, Zimnoch M, Manning AC, Leuenberger M, Uglietti C, Dolman AJ, Ciais P, Heimann M, Tans PP. 2010. Seven years of recent European net terrestrial carbon dioxide exchange constrained by atmospheric observations. *Global Change Biol.* **16**: 1317–1337.

Pillai D, Gerbig C, Ahmadov R, Rödenbeck C, Kretschmer R, Koch T, Thompson R, Neininger B, Lavrié JV. 2011. High-resolution simulations of atmospheric CO2 over complex terrain –representing the Ochsenkopf mountain tall tower. *Atmos. Chem. Phys.* **11**: 7445–7464.

Raschendorfer M. 2001. 'The new turbulence parameterization of LM'. *COSMO Newsl.* **1**: 89–97. http://www.cosmo-model.org/; accessed 22 April 2017.

Ryan MG. 1991. Effects of climate change on plant respiration. *Ecol. Appl.* **1**: 157–167.

Sarrat C, Noilhan J, Dolman AJ, Gerbig C, Ahmadov R, Tolk LF, Meesters AGCA, Hutjes RWA, Ter Maat HW, Pérez-Landa G, Donier S. 2007. Atmospheric CO2 modeling at the regional scale: An intercomparison of five meso-scale atmospheric models. *Biogeosciences* **4**: 1115–1126.

Sarrat C, Noilhan J, Lacarrere P, Ceschia E, Ciais P, Dolman A, Elbers JA, Gerbig C, Gioli B, Lauvaux T, Miglietta F, Neininger B, Ramonet M, Vellinga O, Bonnefond JM. 2009. Mesoscale modelling of the CO2 interactions between the surface and the atmosphere applied to the April 2007 CERES field experiment. *Biogeosciences* **6**: 633–646.

Satar E, Berhanu T, Brunner D, Henne S, Leuenberger M. 2016. Continuous CO2/CH4/CO measurements (2012–2014) at Beromünster tall tower station in Switzerland. *Biogeosciences* **13**: 2623–2635.

Schaap M, Roemer M, Sauter F, Boersen G, Timmermans R, Builtjes PJH, Vermeulen AT. 2005. 'LOTOS-EUROS: Documentation', TNO report 2005/297. Apeldoorn, The Netherlands.

Schneider W, Bott A. 2014. On the time-splitting errors of one-dimensional advection schemes in numerical weather prediction models; a comparative study. *Q. J. R. Meteorol. Soc.* **140**: 2321–2329.

Seibert P, Beyrich F, Gryning S, Joffre S, Rasmussen A, Tercier P. 2000. Review and intercomparison of operational methods for the determination of the mixing height. *Atmos. Environ.* **34**: 1001–1027.

Shrestha P, Sulis M, Masbou M, Kollet S, Simmer C. 2014. A scale-consistent terrestrial systems modeling platform based on COSMO, CLM, and ParFlow. *Mon. Weather Rev.* **142**: 3466–3483.

Šimůnek J, Suarez DL. 1993. Modeling of carbon dioxide transport and production in soil: 1. Model development. *Water Resour. Res.* **29**: 487–497.

Smallman TL, Moncrieff JB, Williams M. 2013. WRFv3. 2-SPAv2: Development and validation of a coupled ecosystem–atmosphere model, scaling from surface fluxes of CO2 and energy to atmospheric profiles. *Geosci. Model Dev.* **6**: 1079–1093.

Suarez DL, Šimůnek J. 1993. Modeling of carbon dioxide transport and production in soil: 2. Parameter selection, sensitivity analysis, and comparison of model predictions to field data. *Water Resour. Res.* **29**: 499–513.

Sulis M, Langensiepen M, Shrestha P, Schickling A, Simmer C, Kollet SJ. 2015. Evaluating the influence of plant-specific physiological parameterizations on the partitioning of land surface energy fluxes. *J. Hydrometeorol.* **16**: 517–533.

Ter Maat HW, Hutjes RWA, Miglietta F, Gioli B, Bosveld FC, Vermeulen AT, Fritsch H. 2010. Simulating carbon exchange using a regional atmospheric model coupled to an advanced land-surface model. *Biogeosciences* **7**: 2397–2417.

Thornton PE, Rosenbloom NA. 2005. Ecosystem model spin-up: Estimating steady state conditions in a coupled terrestrial carbon and nitrogen cycle model. *Ecol. Modell.* **189**: 25–48.

Thornton PE, Zimmermann NE. 2007. An improved canopy integration scheme for a land surface model with prognostic canopy structure. *J. Clim.* **20**: 3902–3923.

Tolk LF, Peters W, Meesters AG, Groenendijk M, Vermeulen AT, Steeneveld GJ, Dolman AJ. 2009. Modelling regional scale surface fluxes, meteorology and CO2 mixing ratios for the Cabauw tower in the Netherlands. *Biogeosciences* **6**: 2265–2280.

Uebel M. 2016. 'Simulation of mesoscale patterns and diurnal variations of atmospheric CO2 mixing ratios with the model system TerrSysMP-CO2', PhD thesis. Rheinische Friedrich-Wilhelms-Universität: Bonn, Germany.

Uebel M, Bott A. 2015. Mesoscale air transport at a midlatitude squall line in Europe –a numerical analysis. *Q. J. R. Meteorol. Soc.* **141**: 3297–3311.

Valcke S. 2013. The OASIS3 coupler: A European climate modelling community software. *Geosci. Model Dev.* **6**: 373–388.

van der Molen MK, Dolman AJ. 2007. Regional carbon fluxes and the effect of topography on the variability of atmospheric CO2. *J. Geophys. Res.* **112**: D01104. https://doi.org/10.1029/2006JD007649.

Wegener O. 2008. *Untersuchung des Einflusses des Klima-wandels auf die CO2-Freisetzung aus Böden ausgewählter hessischer Dauerbeobachtungsflächen –Abschlussbericht*. Hessisches Landesamt für Umwelt und Geologie (HLUG) and AGROFOR Consulting: Wettenberg, Germany. http://www.hlnug.de/static/klimawandel/inklim_plus/dokumente/berichte/boden.pdf (accessed 9 May 2017).

Weihermüller L, Graf A, Herbst M, Vereecken H. 2013. Simple pedotransfer functions to initialize reactive carbon pools of the RothC model. *Eur. J. Soil Sci.* **64**: 567–575.

Zhang D, Hui D, Yiqi L, Zhou G. 2008. Rates of litter decomposition in terrestrial ecosystems: Global patterns and controlling factors. *J. Plant Ecol.* **1**: 85–93.